

# Mechanical Characterization and Numerical Validation of Materials Derived from Organic Composites

Submitted by:  
**Sebastián Andrés Hurtado Siña**



Escola Tècnica Superior d'Enginyers de Camins, Canals i Ports de Barcelona  
Universitat Politècnica de Catalunya

Master Thesis

Advisors:

**Director: Prof. Lucia G. Barbu.**  
**Director: Dr. Alejandro Cornejo.**  
**Co-director: Edgar Aneas Moreno.**

September, 2022

**Mechanical  
Characterization and Numerical  
Validation of Materials Derived from  
Organic Composites**

September, 2022

Universitat Politècnica de Catalunya  
c/ Jordi Girona 1-3, 08034 Barcelona  
[www.upc.edu](http://www.upc.edu)

# Agradecimientos

Quiero agradecer a mis profesores Alejandro y Lucia por el apoyo que me brindaron en este trabajo y por confiar en mí, siempre dispuestos a resolver dudas y entregándome un sin fin de conocimientos. También agradecer a mi familia por el apoyo desde Chile, la distancia no fue impedimento para sentirlos cerca y agradecer a mi pareja Alicia y mis amigos por estar conmigo como una segunda familia.



# Resumen

Los materiales compuestos son una de las soluciones más importantes en el desarrollo de nuevas tecnologías, son ampliamente utilizados en grandes industrias con requerimientos muy exigentes. Estos materiales compuestos utilizados actualmente tienen el problema de tener altos valores de residuos y altos costos energéticos en su producción que motivan el uso de nuevas soluciones materiales, como los compuestos reforzados, especialmente con materiales orgánicos, debido a su capacidad de reciclaje, biodegradabilidad, menor costo energético y producción económica. El uso de este tipo de compuestos presenta una alta barrera de entrada, la confiabilidad de sus características mecánicas para el diseño mecánico.

En este trabajo se caracteriza numéricamente el comportamiento mecánico de dos probetas de materiales compuestos reforzados con fibras orgánicas utilizando la teoría de Serial-Paralelo rule of mixture (SP-RoM), los modelos son calibrados en base a un arduo trabajo iterativo que se contrasta con resultados experimentales encontrados en la bibliografía.

Dentro de la información tratada en este documento se encontrará un resumen de la importancia de estudiar numéricamente este tipo de materiales compuestos y poder caracterizarlos correctamente para su utilización en el diseño mecánico, para esto se realizaron una serie de simulaciones 3D estáticas y no lineales que consideran daño en la matriz y fibra de dos compuestos reforzados por fibras naturales: el primero de resina de poliéster reforzada con fibra Jowar larga y orientada y otra con hormigón espumado con fibra corta de henequén no orientada.

Se realizó un trabajo iterativo para estudiar las propiedades de los materiales y su respuesta mecánica, teniendo en cuenta parámetros como la energía de fractura, Reglas de fluencia y solucionadores como Newton-Raphson y Arc-Length. Finalmente se logra calibrar y caracterizar numéricamente los materiales en base a datos experimentales de ensayos de tensión, compresión y flexión encontrados en la bibliografía.



# Abstract

Composite materials are one of the most important solutions in the development of new technologies, they are widely used in large industries with very demanding requirements. Composite materials currently used have the problem of having high waste values and high energy costs in its production that motivate the use of new material solutions, such as reinforced composites, especially with organic materials, due to their recycling capacity, biodegradability, lower energy cost and economic production. The use of this type of compound presents a high barrier to entry, the reliability of its mechanical characteristics for mechanical design.

In this work, the mechanical behavior of two specimens of composite materials reinforced with organic fibers is numerically characterized using the Serial-Parallel rule of mixture (SP-RoM) theory, the models are calibrated based on an arduous iterative work that is contrasted with experimental results found in the literature.

Within the information discussed in this document you will find a summary of the importance of numerically studying this type of composite materials and being able to characterize them correctly for their use in mechanical design, for this a series of static and non-linear 3D simulations were carried out that consider Damage to the matrix and fiber of two compounds reinforced by natural fibers: one made of polyester resin reinforced with long and oriented Jowar fiber and the other made with foamed concrete with short and no oriented Henequen fiber.

An iterative work is carried out to study the properties of materials and their mechanical behavior, taking into account parameters such as fracture energy, rule of flow and solvers such as Newton-Raphson and Arc-Length, where finally it is possible to calibrate and numerically characterize the materials. based on experimental data from tension, compression and bending tests found in the literature.



*"Los intelectuales  
resuelven problemas,  
los genios los previenen"*



# Contents

<b>1</b>	<b>Introduction</b>	<b>1</b>
1.1	Motivation . . . . .	1
1.2	Objetives . . . . .	2
1.2.1	General objetives . . . . .	2
1.2.2	Specific objetives . . . . .	2
1.3	Contamination by composite materials . . . . .	3
1.3.1	Recycling problem . . . . .	3
1.3.2	Health risks of epoxy resins in composite materials . . . . .	5
1.4	Organic composite materials . . . . .	6
1.4.1	Recyclability of organic composite materials . . . . .	6
<b>2</b>	<b>State of the Art</b>	<b>9</b>
2.1	Composite materials . . . . .	9
2.1.1	Particle reinforced composites . . . . .	9
2.1.2	Fiber reinforced composites . . . . .	10
2.1.3	Structural composites . . . . .	11
2.2	Organic fiber for composite materials . . . . .	11
2.3	Finite element modeling of composite materials . . . . .	14
<b>3</b>	<b>Modeling Using FEM</b>	<b>19</b>
3.1	Introduction to FEM . . . . .	19
3.2	FEM formulation in 3D . . . . .	21
3.2.1	Displacement, strain and stress field . . . . .	21
3.2.2	Isotropic damage model . . . . .	22
3.2.3	Principle of virtual work in 3D . . . . .	24
3.2.4	Finite elements formulation . . . . .	24
3.3	Solving the system of equations . . . . .	29
3.3.1	Newton-Raphson Method . . . . .	29
3.3.2	Response control algorithms – “Arc-Length” . . . . .	31
<b>4</b>	<b>Serial-Parallel Rule of Mixtures (SP-RoM)</b>	<b>35</b>
4.1	Serial-Parallel Rule of Mixtures Theory . . . . .	35
4.2	Formulation of Serial-Parallel Rule of Mixtures Theory . . . . .	36
<b>5</b>	<b>Numerical Characterization of Organic Composite Materials</b>	<b>47</b>
5.1	Numerical characterization of polyester resin specimen reinforced with jowar fiber . . . . .	48

5.1.1	Experimental tension test . . . . .	48
5.1.2	Results of the numerical characterization . . . . .	49
5.1.3	Theoretical and numerical characterization of bending test . . . . .	52
5.1.4	Analysis of results . . . . .	54
5.2	Numerical characterization of Foamed Concrete specimen reinforced with Henequen fiber . . . . .	55
5.2.1	Composite material characteristics . . . . .	55
5.2.2	Experimental compression and tension tests. . . . .	56
5.2.3	Results of the numerical characterization of compression . . . . .	58
5.2.4	Results of the numerical characterization in tension . . . . .	61
5.2.5	Analysis of results . . . . .	63
<b>6</b>	<b>Conclusions and Future work</b>	<b>67</b>
6.1	Conclusions . . . . .	67
6.2	Future work . . . . .	69

# List of Figures

2.1	Schematic 3D views of dispersion and distribution of particulate reinforcements in composites [18]. . . . .	10
2.2	Diagrams of the structures of the most used composite materials [40]. . . . .	11
2.3	Schematic of the Plane Fiber Approach [31]. . . . .	14
2.4	Schematic of the Woven Fiber Approach [31]. . . . .	15
2.5	Rule of Mixture scheme for composite materials [34]. . . . .	16
3.1	General scheme with stages to develop an FEM analysis. . . . .	20
3.2	Sign criterion for the stresses in a 3-D solid [36]. . . . .	22
3.3	General behaviour of the isotropic damage model [50]. . . . .	23
3.4	Example of a 8-noded hexahedra with linear shape function [36]. . . . .	25
3.5	Example of a generic hexahedra FE and its normalized geometry [36]. . . . .	26
3.6	Newton-Raphson technique scheme 3.8. . . . .	30
3.7	“Arc-Length” spherical path – Detail of the solution search [35]. . . . .	34
3.8	“Arc-Length” spherical path – Progress detail in the solution [35]. . . . .	34
4.1	Flowchart with the strategy to solve the proposed system of equations. . . . .	41
5.1	Specimen with dimensions 6.25x3x80 mm with a mesh of 2,268 nodes. . . . .	50
5.2	Results of the numerical model calibrating the composite material. . . . .	50
5.4	X-axis displacements for different steps of the numerical model. . . . .	51
5.5	First order hexahedral structured mesh with 19,089 nodes. . . . .	52
5.7	Results of bending in Z axis of the numerical model in different steps. . . . .	52
5.8	Scheme and variables of the 3-point bending test. . . . .	53
5.9	Validation of the numerical model with calibrated materials. . . . .	53
5.10	(PFC) specimens: (a) compression test and (b) tension test [41]. . . . .	57
5.11	Briquette samples (dog-bone shape). . . . .	57
5.12	5 mm hexahedral structured mesh with 1331 nodes. . . . .	58
5.14	Z-axis displacements for different steps of the numerical model. . . . .	59
5.15	Results of the numerical model calibrating the composite material. . . . .	60
5.16	Mesh of tetrahedral elements with 7690 nodes . . . . .	61
5.17	Boundary conditions in the numerical model. . . . .	62
5.18	Validation of the numerical model with materials calibrated. . . . .	62
5.20	Damage result at different time steps. . . . .	63



# List of Tables

2.1	Comparison of price per kilogram and mechanical properties of different types of fibers (E: Young’s modulus and S: tensile strength) [5]. . . . .	11
2.2	Major Fiber Source, their production and applications [26]. . . . .	13
5.1	Mechanical properties of composite materials [7]. . . . .	48
5.2	Calculated mechanical properties of component materials. . . . .	49
5.3	Calibrated mechanical properties of calculated component materials. . .	51
5.4	The mixture that was prepared with Portland cement [41]. . . . .	55
5.5	Mechanical properties of component materials [41]. . . . .	56
5.6	Calculated mechanical properties of component materials. . . . .	58
5.7	Calibrated mechanical properties of calculated component materials. . .	60
5.8	Comparison of maximum stress in the different meshes. . . . .	61
5.9	Calibrated mechanical properties of calculated component materials. . .	63
5.10	Fracture energies used in numerical models. . . . .	64

# Chapter 1

## Introduction

### 1.1 Motivation

Composite materials are one of the most important solutions in the development of new technologies, they are widely used in the aeronautical, automotive, construction, etc industries due to the possibility of combining mechanical and chemical properties of various materials, achieving high resistance to lower density than other material solutions.

A relevant example of a widely used composite material is carbon fiber reinforced epoxy resin (CFRP) where its worldwide demand, in the aeronautical industry, increases year after year. The use of this material is expected to increase from 63,500 tons (approximately US \$2.34 billion) in 2016 to 117,000 tons in 2022, corresponding to an annual growth rate of 8.7 %. In other words, by 2050, the aviation sector will generate approximately 500,000 tons of total CFRP waste [16]. Another example is the automotive industry, which widely uses composite materials with common reinforcements such as glass and carbon fiber. The production process and cost of these fibers is high, being US\$1,200±1,800/ton for fiber of glass and the energy associated with a production energy of: 30 GJ/ton. In the case of carbon fiber the cost is US\$12,500/ton and the energy associated with production is: 130 GJ/ton [32].

These high values of waste and energy costs motivate the use of new material solutions, such as reinforced composites, especially with organic materials, due to their recycling capacity, biodegradability, lower energy cost and economic production. The use of this type of compound presents a high barrier to entry, the reliability of its mechanical characteristics and mechanical design. For this reason, this work seeks to expand the numerical study of this type of composite materials, allowing to increase the number of organic composite materials characterized in a numerical calculation software, in this case Kratos Multiphysics [37, 12], demonstrating that it is possible to use them in the design of solutions of engineering.

## 1.2 Objectives

### 1.2.1 General objectives

This thesis explores the possibilities and capabilities of numerical modeling in the field of organic composite materials. To do this, Perform a structural Finite Element Analysis (FEA) of two composite materials reinforced by organic fibers that allow establishing a mechanical characterization of the properties of these composites, which are obtained from experimental studies in the literature. The results of the numerical models based on the serial-parallel and parallel mixing theory (SP-RoM) are compared with the curves of the traction, compression and bending tests carried out on the study specimens.

### 1.2.2 Specific objectives

Besides the mentioned general objectives, this thesis aims to:

- Being able to understand, based on a literature review, the importance of organic composite materials as a solution to widespread pollution and the high manufacturing costs of conventional composite materials in the global industry.
- Study the complex modeling of organic composite materials, considering mainly oriented long fiber and dispersed short fiber reinforcements.
- Perform an optimal calibration of composite materials based on experimental results found in the literature, understanding the difficulties of establishing the fracture energy parameters and the mechanical properties of the component materials.
- Carry out the numerical characterization using Kratos multiphysics with the Serial Paralel Rule of mixture theory (SP-RoM) of an organic compound made up of a polypropylene resin matrix reinforced with Jowar Unidirectional long natural fibers, which was tested with tensile and bending specimens according to the bibliography.
- Carry out the numerical characterization using Kratos Multiphysics with the Paralel Rule of mixture theory (P-RoM) of an organic composite formed by a matrix of foamed concrete reinforced with short natural disperse fibers from Henequen, which was tested with tensile and compression specimens according to the bibliography.

## 1.3 Contamination by composite materials

This section describes the problems that exist in the manufacture and use of traditional composite materials in the industrial world. The pollution of the environment, the energy expenditure in its manufacture and the high cost of recycling methods are aspects of paramount importance when working with this type of materials.

Materials based on epoxy resins and reinforced with carbon fiber, usually called CFRP, have been widely used for weight reduction in the aeronautical industry. For example the Boeing 787 has used up to 50 % weight of CFRP materials in the body structure. Global demand is increasing year on year and carbon fibers are expected to increase from 63,500 tons (approximately US \$2.34 billion) in 2016 to 117,000 tons in 2022, corresponding to an annual growth rate of 8.7% [16]. By 2050, the aviation sector will generate approximately 500,000 tonnes in total of CFRP waste from the production phase and end of life of aircraft [16].

Other industries as important as the automotive industry widely use traditional composite materials with common reinforcements such as glass and carbon fiber, even though the production process and the cost of these fibers is high. This kind of material can cost US\$1,200±1,800/tonne for glass fiber. and a production energy of: 30 GJ/ton, in the case of carbon fiber a cost of US\$12,500/ton is associated and a production energy of 130 GJ/ton.

For this reason and considering the large amount of composite material used by the automotive industry, other options are proposed to reduce energy expenditure and costs. One of them is the reinforcement with natural fibers, which have a production cost of: US\$200±1000/tonne and a production energy: 4 GJ/tonne [32].

### 1.3.1 Recycling problem

The large number of compositions and types of composite materials requires that there be a classification when processing their recycling, since each one will have a different system to be worked on.

One of the most common composite materials is the one with a thermoset matrix, regardless of the type of fiber with which it is reinforced. This type of composite material has 3 types of recycling processes, where each has advantages and disadvantages [23]:

- **Mechanical recycling:** it is the most mature method, based on reducing the size of waste from fine powder to bigger fibrous recyclates. These products can be used as fillers in short fibre composites, but they have a low market value.
- **Thermal recycling:** these methods aim to break down the matrix and recover the fibres. Mainly are based on pyrolysis effect and in fluidized bed recycling.

- **Chemical recycling:** it aims to decompose the CFRP and recover the fibres by means of different chemical methods such as solvolysis, electrochemical or catalytic depolymerisation methods, but with a huge energy expenditure.

In addition to what was mentioned above, these composite materials usually have a series of extra difficulties which are listed below [23]:

- Thermosetting matrix composite materials cannot be reprocessed by recast processes.
- Scraps from cuttings in part manufacturing are often contaminated with metal inserts or stiffeners.
- The high content and types of reinforcements, inorganic minerals such as fiber-glass, greatly hinder the separation processes of materials in the composite.

Another problematic aspect in any recycling process of composite materials is that the series of operations that make up the recycling process have to be all successful, this is important because each of these operations depends on another, this implies that the failure of any one in the chain implies that the global recycling process cannot be completed.

If we consider a common recycling process of composite materials, according to J.Manso [29], we can refer to the following stages:

- Availability of waste from composite materials: They can be products or parts that have already completed their useful life or waste products produced during the manufacturing processes.
- Collection, transport and separation of waste: Especially in the recycling of used parts, the collection, separation and transport to recycling centers is a complicated stage due to the presence of other by-products or contaminants that can reduce the efficiency or purity of the process for obtaining the recycled material. The size of the products to be recycled can also be a problem when transporting them, as is the case with aviation by-products or wind turbine blades, which, due to their size, require prior treatment on site before transport.
- Reprocessing: The application of physical processes (mechanical), chemical, thermal technologies, or a combination of both, depending on the type of material, constitutes the most important recycling process. Currently, there is a great demand for separation and recovery processes that are efficient and meet the requirements established by the authorities and the quality demanded by the companies for the final material.
- Market for recycled products: It is essential that recycled products have a demand in the market, so that the entire recycling process has an economic livelihood. The quality of the product obtained must be adequate to meet the standards of the companies and its prices must be competitive compared to virgin products.

Many of these difficulties in the recycling of composite materials are applicable to organic composite materials, but it must be emphasized that organic materials that are part of the composite have a considerably shorter degradation time. Organic composites that reach the environment without a recycling process will disintegrate much faster than the classic compounds used in industry due to their natural nature. It is also interesting to highlight processes such as composting or biofuel production because they take on greater relevance in purely organic composite materials. All these aspects will be reviewed in the section 1.4.1.

### 1.3.2 Health risks of epoxy resins in composite materials

In the epoxy resins widely used as a matrix in composite materials, we can find Bisphenol A (BPA) [4] as a constituent. An organic compound with two phenol functional groups that is considered an endocrine disruptor, causing health problems for people and animals due to its degradation in nature. The highest percentage of BPA is used as a component of the polycarbonate (74% of the total amount of produced BPA) and the epoxy resins (nearly 20%). As a result of the mass production, a large number of derivatives of BPA are released into the environment, which consequently leads to increasing pollution and contamination of the soil and groundwater [17].

Due to its phenolic structure (BPA) has been shown to interact with estrogen receptors and to act as agonist or antagonist via endocrine receptor (ER). Therefore, (BPA) has been shown to play a role in the pathogenesis of several endocrine disorders including female and male infertility, precocious puberty, hormone dependent tumours such as breast and prostate cancer and several metabolic disorders including polycystic ovary syndrome [4].

It is also associated that concentrations of (BPA) detected in the urine are related to type 2 diabetes, problems with liver enzymes and cardiovascular problems [22]. This type of health problems grow due to multiple exposures of (BPA) with the body and one of them is the degradation of waste produced by the manufacturing processes of composite materials with epoxy resins and the large percentage of composite materials that are not recycled in industry.

Being able to reduce the use of epoxy-based matrices is essential to mitigate the risk that human beings have when exposed to this component. Composite materials with organic matrices are a solution to reduce the kilograms of epoxy used in world industry and replace this resin, especially in structures that have a relatively low useful life. Authors such as O. Donnell, M.A. Dweib and R.P. Wooles [2] say that it is possible to replace, for some applications, epoxy matrices by matrices based on natural resins coming from trees or plants. An example is the base structures of motor rates which are usually not recycled and end up degrading in the environment.

## 1.4 Organic composite materials

There are several definitions of biocomposites or organic compounds; The most accepted definition that biocomposites are composite materials in which at least one of the constituents is derived from natural resources. This corresponds well with the definition set out in the CEN standard. This definition offers countless possibilities for the design of composite formulations, ranging from petroleum-based to biobased polymer matrices, from glass fiber to natural fiber reinforcement, and from virgin to recycled polymers. Important for all biocomposites is that their susceptibility to abiotic degradation, water absorption and biodegradation processes must be considered to guarantee their structural and functional stability during their useful life [8].

This implies that for an organic compound we can make the distinction into three possible global groups, the first is the use of an organic matrix and an inorganic reinforcement, on the other hand we can have an inorganic matrix with organic reinforcements and finally a composite material where its entirety is organic. Each of these types of compounds vary in their physical properties, manufacturing methods, and recycling processes.

### 1.4.1 Recyclability of organic composite materials

One of the most important aspects of this topic is that there are two ways to work with waste or disused pieces of organic composite materials. One is directly related to biodegradability and the other to the common recycling of this type of material.

Each organic composite material may have a different degradation or recyclability process, because it depends directly on the type of matrix and fiber it is composed of. An example is that established by Bourmaud [8, 9], which has shown that PP and vegetable fiber compounds are recyclable following the European directive 2000/53/CE, which imposes the reuse/recycling of at least 95 % of the weight of a vehicle used before 2015. The mechanical and thermophysical behavior of PP/hemp or sisal composite after seven injection cycles showed a small decrease in tensile strength and modulus of the recycled composite for the seventh time, which could be compensated by adding fibers /additional polymers in proportion to recycled materials

Another example is the recycling of PP-based composites reinforced with rice hulls or kenaf fibers is promising because their properties remain almost unchanged after recycling processes. In addition, recycled composites have potential use as building materials for interior applications because the flexural strength and modulus of these materials are comparable to conventional formaldehyde-based wood medium-density fiberboard. Furthermore, PP-based composites were less sensitive to processing cycles than PLA-based composites [46].

These examples show that the recyclability of organic compounds reinforced with natural filler (based on a synthetic or biopolymeric thermoplastic matrix) is usually guaranteed up to several reprocessing cycles to preserve the mechanical properties. Multiple processing can even improve interfacial adhesion between fillers and matrix, resulting in a reported increase in thermal stability in reprocessed biocomposites. However, different degradation effects can occur due to the repeated recycling of biocomposites, such as the reduction of fiber length [51].

All this information, added to what has been discussed in previous chapters, allows us to understand the importance of being able to use organic replacements for matrices, reinforcements or both in the composite materials industry. The reduction of production costs, ease of degradation and recycling, new options for reuse as bio-fuels and lower health risks are reasons to study and generate more knowledge about these types of composites.



# Chapter 2

## State of the Art

### 2.1 Composite materials

A composite material is a system made up of the combination of two or more micro or macroconstituents that differ in form and chemical composition, which are essentially insoluble in each other. These constituents, depending on their length scale, can be considered as microstructures ( $10^{-7}$  m to  $10^{-4}$  m), macrostructures (greater than  $10^{-3}$ ) and nanostructures (less than  $10^{-8}$ ). The importance of composite materials in engineering is gigantic, since it is possible to combine the properties and performance of the constituent materials when the composite material is correctly designed and manufactured. [5].

Most composite materials are made up of two or more phases, a continuous matrix surrounding the other phases called dispersed phases and classified based on their microstructure or geometry. The microstructure of the dispersed phase includes the shape, size, distribution, and orientation of the particles. When the proportions of matrix material and disperse material are given, a clear distinction must be made between weight and volume ratios since the densities of these phases can be very different.

Based on the criteria of the nature of the microstructure of the dispersed phase for the classification of composite materials, three large groups can be established:

#### 2.1.1 Particle reinforced composites

They are classified into materials reinforced with large particles and others consolidated by dispersion. The term “large” is used to indicate the interactions between the matrix and the particles at a macroscopic level. The most common large particle reinforced composite material is concrete.

Particles can have a wide variety of geometry, but they tend to have approximately the same dimensions in all directions (equiaxial), which is the big difference with fibers. The reinforcement is more effective the smaller the size of the particles and the more homogeneously distributed they are in the matrix. The mechanical properties improve with the increase in the particle/matrix ratio [5].

Within the range of particulate reinforcements we can find ceramic powders, steel or aluminum powders, among others. Regardless of the type of reinforcement particle, it is extremely important that the dispensing is adequate. Author G. Zhang et al [18] comment that particle contact points in aggregates will provide crack initiation sites or act to enhance crack propagation, leading to premature composite failure when the composite is under mechanical stress. Ideally, the particles present in the compound should be in a dispersed state. Therefore, specially designed processing equipment and/or good manufacturing procedures are often required.

They also add that generally, there is a critical amount of particle reinforcement for the composite material, only above which the desired properties for the composite material can be obtained. In such a situation of highly charged polymers, the processing of the compounds becomes a challenge. [18].

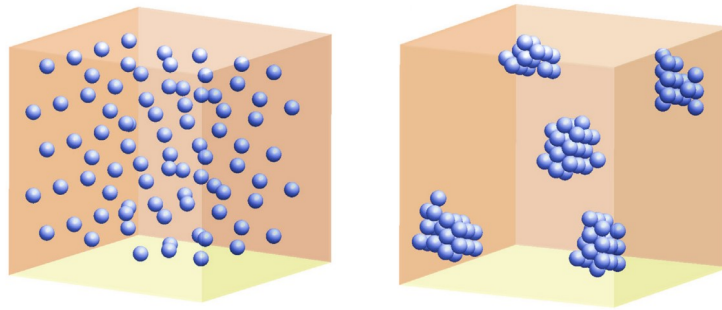


Figure 2.1: Schematic 3D views of dispersion and distribution of particulate reinforcements in composites [18].

### 2.1.2 Fiber reinforced composites

These are the widely known composite materials for their high mechanical performance and the high added value of the final material. The disperse phase consists of fibers which is a highly anisotropic microstructure. These fibers can be of different thickness and length, generating subdivisions in this classification, being long or short fiber matrix materials.

Author G. Zhang et al [18] suggests that for long-fiber composites, fiber arrangement such as fiber orientation, fiber stacking pattern, and the angle and packing sequence of fiber-reinforced sheets is a critical factor affecting the performance of long-fiber reinforced composites. For short-fiber composites, the fiber length, aspect ratio, and fiber orientation are key influencing factors. While the fiber length affects the load transfer between short fibers and the matrix locally, fiber orientation affects the macroscopic properties of the composite. The random orientation or alignment in one direction of short fibers in composites results in isotropic or anisotropic materials. However, isotropic short-fiber composites (i.e., those with randomly oriented short fibers) can become “anisotropic” upon unidirectional tension when the fibers are “forced” aligned to some extent due to the effect of the elongational flow.

The modulus of elasticity does not change with the size of the material, it only depends on the nature of the forces that join the atoms, the mechanical resistance does change with the shape of the sample. Smaller (narrower) specimens have comparatively higher strengths. The explanation is due to the fact that the probability of finding defects in the macro-microscopic scale that are the main responsible for the appearance of the crack and fracture decreases [5].

The high added value of these materials can be verified in Table 2.1, where the values per kilogram of different materials are given. Variations in Young's modulus and tensile strength for different types of materials are also given in the same Table 2.1.

Material	Price (Euro/Kg)	Density (g/cc)	E (GPa)	S (GPa)
Concrete	0.04	2.8	45	0.005
Steel	0.5	7.8	210	2.8
Aluminum	1.3	2.7	70.5	0.045
Fiberglass S	18	2.48	82	3.0
Carbon Fiber HS	30	1.7	200	4-6
Kevlar49	30	1.5	140	3.0

Table 2.1: Comparison of price per kilogram and mechanical properties of different types of fibers (E: Young's modulus and S: tensile strength) [5].

### 2.1.3 Structural composites

They present a combination of homogeneous materials and the properties depend more on the design geometry of the structural elements than on the nature of the constituent materials. These material layers are usually laminar or sandwich and are highly anisotropic. For example, plywood, copper and aluminum honeycomb for heat exchangers, corrugated cardboard.

## 2.2 Organic fiber for composite materials

Nowadays, the natural plant fiber form is an interesting option for the most widely applied fiber in the composite technology. Natural fibers have a good potential as a substitute for petroleum or nonrenewable source material in many applications. The

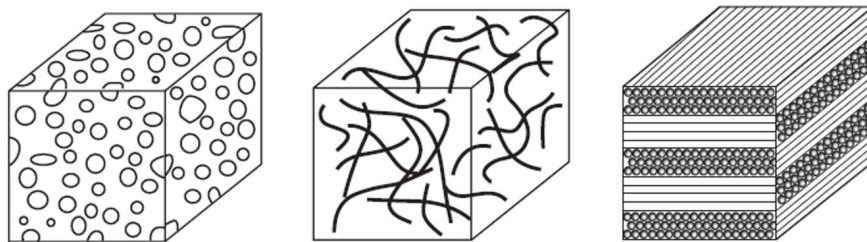


Figure 2.2: Diagrams of the structures of the most used composite materials [40].

development of environmentally friendly green composites is because of natural fiber's biodegradability, light weight, relative cheapness, high specific strength, natural abundance, plentiful supply, and swift replenishing ability (compared to nonrenewable products), and these characteristics are the strongest arguments to utilize them in the composites [39].

For these reasons, much research has been conducted to study the exploitation of natural fibers as load-bearing constituents in composite materials. From an economic development and sustainability perspective, natural fiber reinforced composites provide an opportunity to develop forestry and an agriculture-based economy (nonfood sector). Furthermore, in comparison with the most common synthetic reinforcing fibers, natural fibers require less energy to produce and are the ultimate green products. The global natural fiber composite market reached \$2.1 billion in 2010, with a compound annual growth rate of 15% in the last five years. The automotive and construction industries were the largest segment among all natural fiber composite applications [39].

There are several types of natural fibers available for use as reinforcement in the development of natural fiber reinforced composites. Some natural fibers that give excellent results as reinforcement are pineapple leaf fiber, bamboo, jowar, banana, jute, hemp, flax, sisal, etc. Within the wide range of natural fibers, we can classify them into six types [26]: a) Cane fibers: these fibers include wheat, corn and rice. b) Leaf fibers: Abaca, Sisal and Pineapple are leaf fibers. c) Bast fibres: Jute, flax, hemp, ramie and kenaf are examples of bast fibres. d) Seed fibers: These include coconut fiber, cotton and kapok. e) Core fibres: Kenaf, hemp and jute are examples of these fibres. f) All other types: Includes wood and roots. Table 2.2 shows the main source of natural fiber, its production in the world and the main applications.

We can highlight the Jowar fiber, due to its low density compared to other natural fibers, it can be widely used in the manufacture of light materials for the housing sector, the construction of automobile bodies and the packaging industry, etc [26].

As with synthetic fiber reinforcements, physical properties such as length and diameter of the natural fiber also influence the mechanical properties of the composite [38, 1, 52]. Natural fibers having a small diameter have a more positive impact on mechanical properties than fibers with a large diameter [3]. If the fiber length is less than the critical length, this results in a decrease in the stress transfer efficiency between the fiber and the matrix, resulting in lower mechanical properties [33].

The volume percentage of fibers within the composite is also an important factor for the mechanical properties of the final materials. Increasing the percentage of high strength fiber content results in improved mechanical properties. But if the content of high-strength fiber is increased beyond the optimum value, it may cause the deterioration of the mechanical properties [21, 19, 25]. This is because as the fiber content increases, the composition of the matrix decreases, leading to a weaker interfacial bond between the matrix and the composite [3].

S. No	Fiber Source	World Production ( $10^3$ Ton)	Applications
1	Bamboo Fiber	30,000	Commonly used in construction and carpentry industries.
2	Jute Fiber	2,300	Packing, geotextiles, door frames and shutters, building panels, chip board.
3	Kenaf Fiber	970	Mobile cases, insulations, bags, packing materials, animal bedding.
4	Flax Fiber	830	Tennis racket, snowboarding, window frame, decking, fencing, bicycle frame.
5	Sisal Fiber	378	Construction industries such as door, panels, roofing sheets, etc.
6	Hemp Fiber	214	Furniture, electrical, paper industry, textile industry, cordage.
7	Coir Fiber	100	Flush door shutters, mirror casing, filling materials for upholstery, brushes and brooms, ropes and yarns for nets, seat curshions, roofing sheets.
8	Ramie Fiber	100	Packing materials, industrial sewing thread, fishing net, household furnishings and clothing, paper manufacture.

Table 2.2: Major Fiber Source, their production and applications [26].

## 2.3 Finite element modeling of composite materials

The numerical study of composite materials has increased over the years, due to the need to develop models that adequately approximate the mechanical behavior of the matrix assembly and reinforcements that are used. In this work we will focus on some current examples of existing numerical models to approximate this type of materials whose reinforcement is by means of fibers.

According to M.Barschke et al [31], the study of the behavior of fiber-reinforced composite materials usually follows two different approaches. The first is related to a micromechanical aspect, which considers the composite material as a combination of several materials and approximates the average mechanical properties considering the properties of the materials that compose it in a unit cell. The continuous approach considers the composite material as a homogeneous material with uniform average properties throughout its structure and that depends on the percentage that each one uses in the total volume of the material [31].

One of the theories used is the **Classical Laminate Theory [CLT]**, which is based on  $C^1_z$  function theories which assume that the displacement is varying continuously differentiable across the thickness. References like [30] y [47] show a 3-D micromechanical model based on the [CLT] for predicting the elastic behavior of fiber-reinforced materials, mainly textiles. For the simulation of the different layers of the composite material there are 2 approaches [31]:

The **The Plane Fiber Approach** uses Link type elements to simulate the fibers and shell elements to simulate the matrix. In this approach, rigid connections are established between the orthogonal fibers, due to the fact that the vertical and horizontal Link elements use the same nodes. To obtain the correct mass of resin without affecting its moment of inertia, a section of the matrix is modeled in two layers with the fiber in between. To connect the two layers of the resin and the fiber layer, each fiber layer node is coupled at each DOF with the corresponding fiber layer nodes above and below.[31].

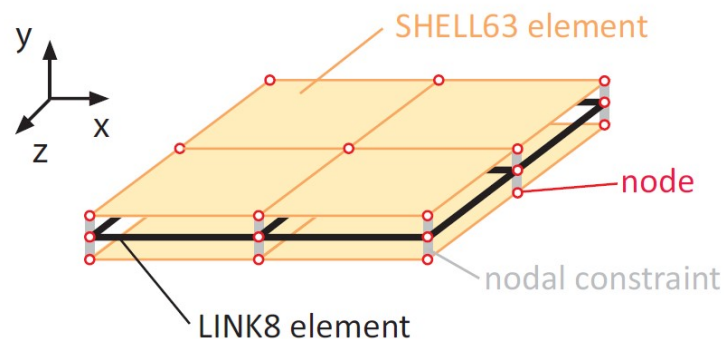


Figure 2.3: Schematic of the Plane Fiber Approach [31].

There is also the **Woven Fiber Approach**, where the resin is divided into layers. To maintain the geometric proportions of the material, the nodes of the Link elements are placed centered between the layers of the solid elements. The required rigid connections between the element nodes, and thus between the fiber and the matrix, are implemented by coupling the corresponding nodes in all degrees of freedom. This model allows more accurate approximations, but with high computational costs compared to the previous model. [31].

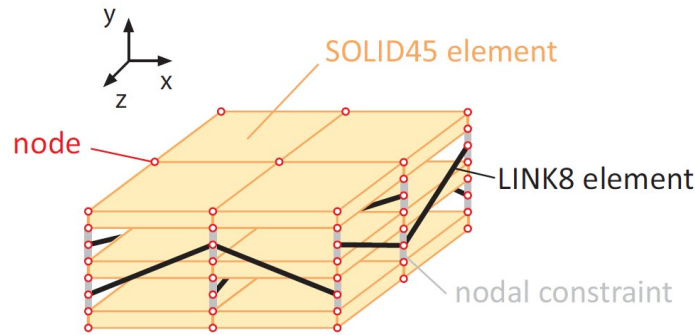


Figure 2.4: Schematic of the Woven Fiber Approach [31].

Another widely used model is **The Serial-Parallel Rule of Mixtures theory**, abbreviated as **[SP-RoM]**, can be defined as a phenomenological homogenization, in which the behavior of the composite material is obtained from the constitutive response of its components. The SP-RoM models the behaviour of the composite by combining the mechanical response of the constituents and its volume participation. [53, 13, 28, 44].

The SP-RoM theory has been the result of the evolution and development of the parallel mixing theory, a theory based on the classical mixing theory, showing a chain of developments fundamental to current theory [10].

The origin of the classical mixing theory is related to the analysis of the micromechanical properties of the compound, through the contribution or volumetric contribution of each component in relation to the complete volume of the compound. In addition to establishing the following foundations [48].

- All components undergo the same strains in the composite (iso-strain condition).
- Each component contributes to the final stress proportionally to its volumetric share in the compound (Figure 2.5).

These hypotheses gave rise to the formulation of the parallel mixing theory, formulated by Car [10, 14], which allowed simulating the non-linear behavior of composite materials.

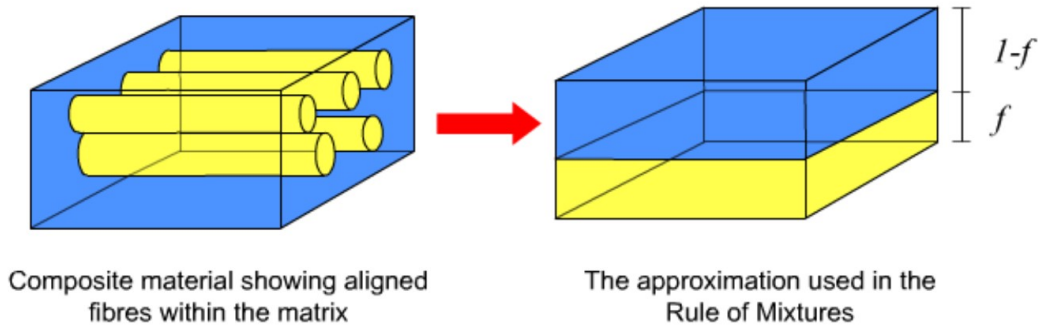


Figure 2.5: Rule of Mixture scheme for composite materials [34].

This theory incorporates in its formulation the ability to couple the linear and non-linear constitutive behavior of a group of component materials, independent of the numerical models used to simulate each of them, for which compatibility conditions are established that expand the foundations of the classical theory of mixing [13, 48].

- Each infinitesimal volume of the composite material contains a finite number of component materials.
- The contribution of each component to the overall behavior of the compound is directly proportional to its volumetric participation in the compound.
- The volume of each component is significantly less than the volume of the compound.
- The different component materials are assumed to be perfectly linked (there is no relative slip between them).
- All components undergo the same strains in the composite (iso-strain condition).

In addition, this theory uses the mean field methodology (MFM) which adds two extra hypotheses [13]:

- The average stresses and strains of each of the components of the composite material are representative of the behavior of the composite.
- The stresses and strains in the composite material are related to the stresses and strains in each component.

With these foundations it is possible to obtain the response of the composite material based on the behavior of its component materials, considering the volumetric participation of each one. The iso-strain condition allows to establish the strain of all the components and using the constitutive equations of each one, we can obtain the individual stresses and in turn these are used to obtain the total stress of the compound.

The limitation of this theory lies in the foundation of the iso-deformation, that is to say that the deformation of each material is the same, an aspect that in reality is not completely fulfilled and that can add a source of error to the behavior of the simulated composite.



# Chapter 3

## Modeling Using FEM

### 3.1 Introduction to FEM

The Finite Element Method (FEM) is a numerical method used in the analysis of structures to give an approximate solution to the constitutive equations that govern the problem. The use of this technique allows to obtain a solution that allows a global vision of the structural behavior. This is fundamental to study the response of complex areas of mechanical designs, for example complete structures with non-intuitive behavior or complex regions to calculate analytically.

The idea of discretization is very old, the mathematical papers on FEA by Schelbach and Courant show the same approach. Earlier, before 1922, also Courant used the finite element ideas in Dirichlet's principle. The FEM we use today involves the contribution of many researchers, namely Turner, Clough, Martin and Topp, Argyris, Babuska, Aziz, Irons, Melosh and many more, like Turner at being perfected the direct stiffness method, Clough coined the term 'Finite Elements', contribution of Irons towards FEA was the introduction of shape functions and patch test. Text books by Hughes and Bathe, Zienkiewicz laid the foundation for further advancement of FEM, and thus the period of 1962–1972 is known as the golden age of FEM [27].

This methodology is based on the concept of FE (Finite Elements). These should be understood as a finite division of the study domain where the structure is analyzed. Depending on the nature of the analysis, FEs can be 1-D (truss elements), 2-D (triangular or quadrilateral elements), or 3-D (tetrahedral or hexahedral elements). For the characterization of the composite material, the use of 3-D elements is necessary, so the formulation presented in this section is the one that will be used for this type of approach [43].

The procedure followed during the performance of a simulation using the FEM can be summarized in the following scheme (Figure 3.1) :

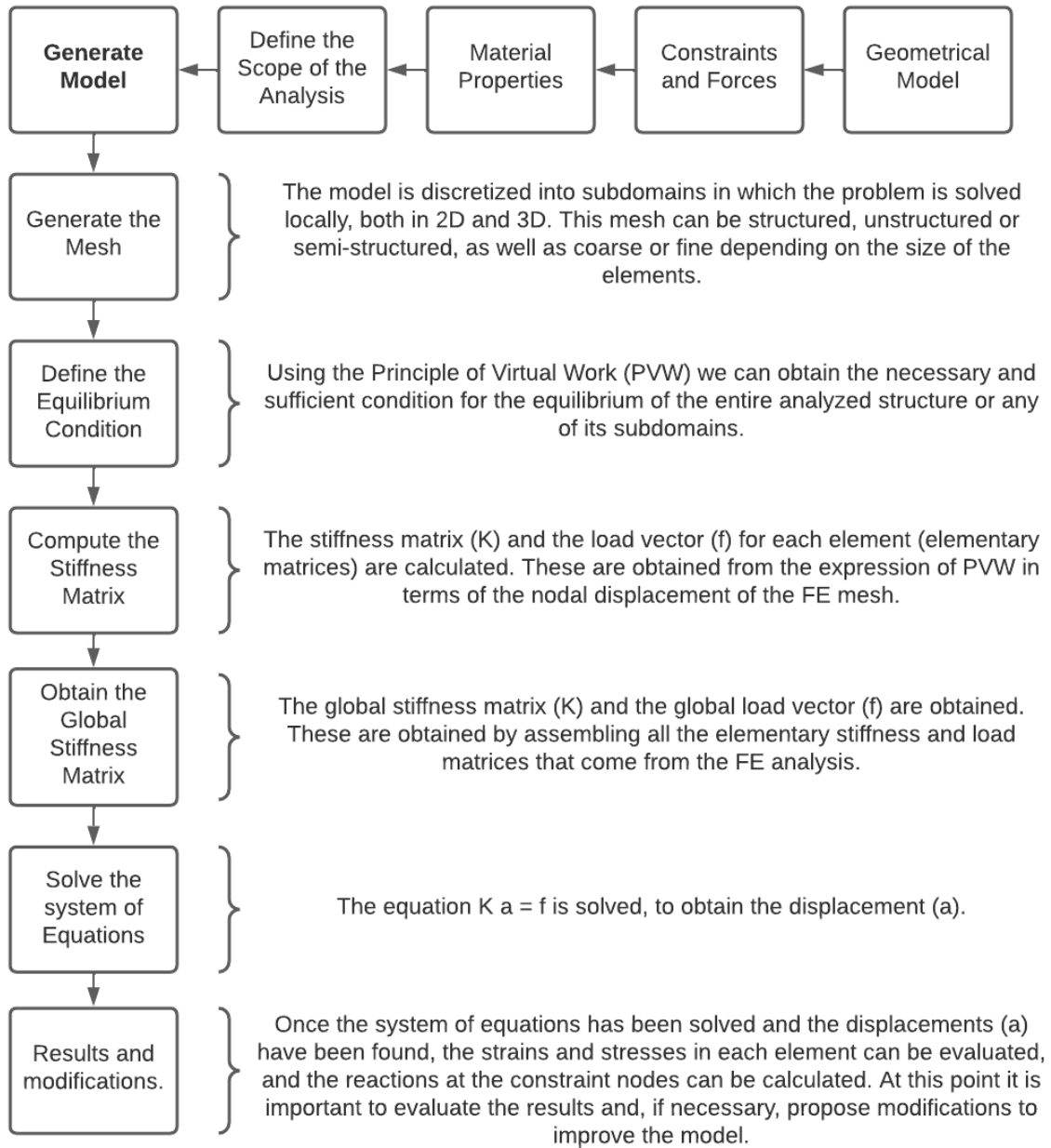


Figure 3.1: General scheme with stages to develop an FEM analysis.

## 3.2 FEM formulation in 3D

### 3.2.1 Displacement, strain and stress field

In the simulation of a solid in 3 dimensions it is necessary to determine the movement of any point belonging to the solid, for this the three components of the displacement vector are described.

$$\mathbf{u} = [u, v, w]^T \quad (3.1)$$

Where  $u$ ,  $v$  and  $w$  are the displacement components of the vector  $\mathbf{u}$  in the directions of a Cartesian reference system  $x$ ,  $y$  and  $z$ , respectively.

Now it is necessary to describe the small strain field, this is done through the six strain components of three-dimensional elasticity:

$$\boldsymbol{\varepsilon} = [\varepsilon_x, \varepsilon_y, \varepsilon_z, \gamma_{xy}, \gamma_{xz}, \gamma_{yz}] \quad (3.2)$$

With:

$$\varepsilon_x = \frac{\partial u}{\partial x}, \varepsilon_y = \frac{\partial v}{\partial y}, \varepsilon_z = \frac{\partial w}{\partial z} \quad (3.3)$$

$$\gamma_{xy} = \frac{\partial u}{\partial y} + \frac{\partial v}{\partial x}, \gamma_{xz} = \frac{\partial u}{\partial z} + \frac{\partial w}{\partial x}, \gamma_{yz} = \frac{\partial v}{\partial z} + \frac{\partial w}{\partial y} \quad (3.4)$$

Where  $\varepsilon_x$ ,  $\varepsilon_y$  and  $\varepsilon_z$  are the normal strains and  $\gamma_{xy}$ ,  $\gamma_{xz}$  and  $\gamma_{yz}$  are the tangential strains. Similarly, the stress field is defined by the six stress components corresponding to the six nonzero strains:

$$\boldsymbol{\sigma} = [\sigma_x, \sigma_y, \sigma_z, \tau_{xy}, \tau_{xz}, \tau_{yz}]^T \quad (3.5)$$

Where  $\sigma_x$ ,  $\sigma_y$  y  $\sigma_z$  are the normal stresses and  $\tau_{xy}$ ,  $\tau_{xz}$  and  $\tau_{yz}$  are the tangential stresses defined according to the sign criterion described in Figure 3.2.

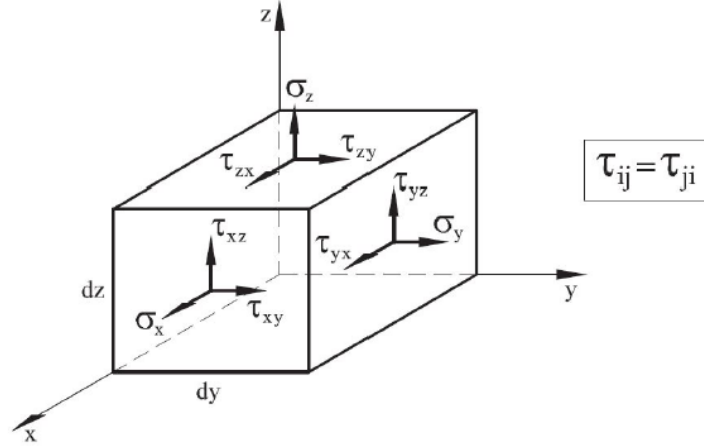


Figure 3.2: Sign criterion for the stresses in a 3-D solid [36].

At this point we have to establish the relationship between the strain and stress fields, this is done through the following constitutive equation. Considering the initial stresses and strains, the relationship is:

$$\boldsymbol{\sigma} = \mathbf{D} (\boldsymbol{\varepsilon} - \boldsymbol{\varepsilon}^0) + \boldsymbol{\sigma}^0 \quad (3.6)$$

As explained in reference [43], the isotropic constitutive matrix ( $\mathbf{D}$ ) depends only on two material parameters, i.e. the Young modulus ( $E$ ) and the Poisson's ratio ( $\nu$ ). Therefore, the symmetric tensor  $\mathbf{D}$  is given by:

$$\mathbf{D} = \frac{E(1-\nu)}{(1+\nu)(1-2\nu)} \begin{bmatrix} 1 & \frac{\nu}{1-\nu} & \frac{\nu}{1-\nu} & 0 & 0 & 0 \\ & 1 & \frac{\nu}{1-\nu} & 0 & 0 & 0 \\ & & 1 & 0 & 0 & 0 \\ & & & \frac{1-2\nu}{2(1-\nu)} & 0 & 0 \\ & & & & \frac{1-2\nu}{2(1-\nu)} & 0 \\ Sym. & & & & & \frac{1-2\nu}{2(1-\nu)} \end{bmatrix} \quad (3.7)$$

### 3.2.2 Isotropic damage model

Taking as reference the explanation of the damage model made by author Cornejo et al [50], we explain how to model the material degradation of the material (non-linear constitutive behaviour) an isotropic damage model have been used, originally developed by Oliver et al [15]. The general behaviour of the model is depicted in Figure 3.3. In this constitutive model, an internal damage variable  $d$  describes the material degradation. This scalar variable ranges from 0 (intact material) to 1 (fully damaged material). The constitutive relation between the strains and stresses is (assuming small strains:  $\det(\mathbf{F}) \approx 1$ ):

$$\boldsymbol{\sigma} = \mathcal{C}_s \boldsymbol{\varepsilon} = (1 - d)\mathcal{C}_0 \boldsymbol{\varepsilon} = (1 - d)\bar{\boldsymbol{\sigma}}, \quad (3.8)$$

Where the effective stress tensor  $\bar{\boldsymbol{\sigma}} = \mathcal{C}_0 \boldsymbol{\varepsilon}$ , the elastic constitutive tensor  $\mathcal{C}_0$  and the secant constitutive tensor  $\mathcal{C}_s = (1 - d)\mathcal{C}_0$  have been introduced.

It is important to note that the isotropic damage model can also be derived from an associated strain energy potential whose definition is [50].

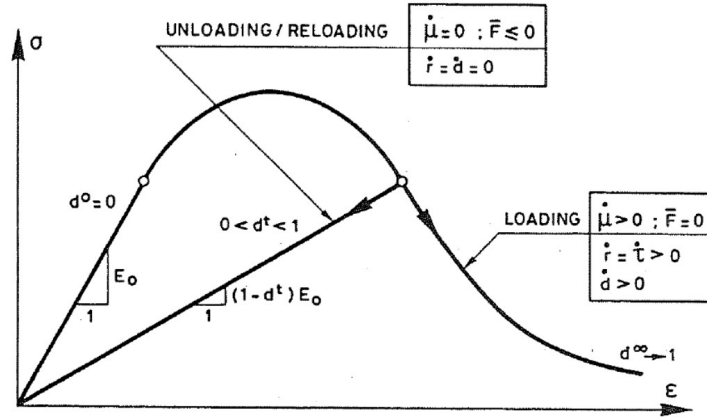


Figure 3.3: General behaviour of the isotropic damage model [50].

$$\Psi(\boldsymbol{\varepsilon}) = \frac{1 - d}{2} (\boldsymbol{\varepsilon} : \mathcal{C}_0 : \boldsymbol{\varepsilon}). \quad (3.9)$$

In order to know whether the material is in elastic or plastic regime, one must define a yield surface and establish a damage criterion such as:

$$\Phi = f(\bar{\boldsymbol{\sigma}}) - \kappa \leq 0 \quad (3.10)$$

Where  $f(\bar{\boldsymbol{\sigma}})$  is the so-called equivalent effective stress whose definition depends on the yield surface of interest (Rankine, Mohr-Coulomb, Simo-Ju, Drucker-Prager, etc.), and  $\kappa$  is the stress threshold (related to the material strength), which each yield surface will define and updated afterwards. In order to see the expressions of  $f(\bar{\boldsymbol{\sigma}})$  and  $\kappa$  of the yield surfaces. The stress threshold  $\kappa$  has to be updated during calculation as [50]:

$$\kappa = \max(\kappa_0, \max(f(\bar{\boldsymbol{\sigma}})_t)) \quad t \in [0, T], \quad (3.11)$$

Which means that the material threshold is the maximum historical equivalent stress achieved if has ever been damaged. This ensures the irreversibility of the damaging process. Once the damage occurs, the internal damage variable  $d$  has to be computed. There are several expressions available for softening and hardening (usual in directional damage in compression), but it has only been considered an exponential softening law for the damage. [15, 50]:

$$d(\bar{\sigma}) = 1 - \frac{\kappa_0}{f(\bar{\sigma})} \exp \left( A \left( 1 - \frac{f(\bar{\sigma})}{\kappa_0} \right) \right) \quad (3.12)$$

In which the  $A$  parameter is determined from the energy dissipated in an uniaxial tension test as [15, 50]

$$A = \left( \frac{G_f \varepsilon}{\hat{l} f_t^2} - \frac{1}{2} \right)^{-1} \geq 0 \quad (3.13)$$

Being  $f_t$  is the tensile strength,  $G_f$  is the specific fracture energy per unit area (taken as a material property) and  $\hat{l}$  is the characteristic length of the element. By using this normalization, the size-effect problem is overcome.

### 3.2.3 Principle of virtual work in 3D

In order to ensure that the equations are in balance, it is necessary to establish the Principle of Virtual Work (PVW), for solids in 3D it is expressed by the following equation:

$$\int \int \int_V \delta \varepsilon^T \boldsymbol{\sigma} dV = \int \int \int_V \delta u^T b dV + \int \int_A \delta u^T t dA + \sum_i \delta a_i^T F_i \quad (3.14)$$

Where the integrals are in the volume and in the area of the solid respectively, in addition  $\delta \varepsilon$  corresponds to the virtual deformation and  $\delta u$  to virtual displacement. Also this equation involves the body forces ( $b$ ), surface tractions ( $t$ ) and point charges ( $F$ ) acting at nodes  $i$ .

### 3.2.4 Finite elements formulation

After establishing the equilibrium described in the previous section, it is possible to work out the FEM formulation. In this case, hexahedral elements are used to present the finite element formulation.

There are many types of hexahedral elements, for this reason the formulation of the specific 8-node linear hexahedral element is described (Figure 3.4). For this we begin by describing the Shape Functions of this element ( $N_i^{(e)}$ ). These functions are interpolation polynomials over the domain of each element in the FE mesh that take the value one at node  $i$  and 0 at the rest of the nodes, for this reason the equation must satisfy  $u(x_i) = u_i^{(e)}$  [43].

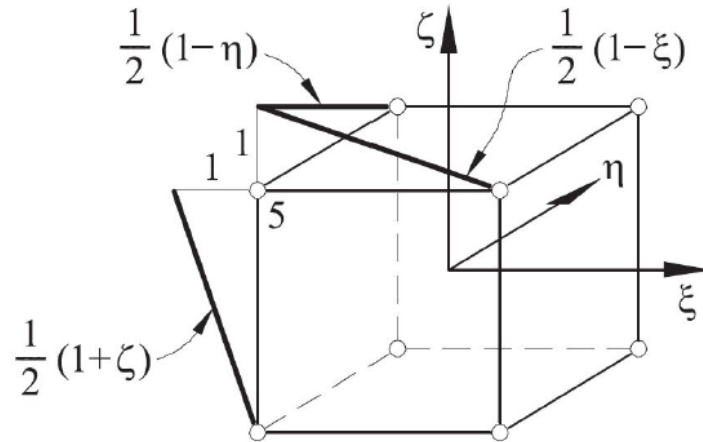


Figure 3.4: Example of a 8-noded hexahedra with linear shape function [36].

For this type of hexahedral element the nodal shape function can be written as:

$$N_i(\xi, \eta, \zeta) = \frac{1}{8}(1 + \xi_i\xi)(1 + \eta_i\eta)(1 + \zeta_i\zeta) \quad (3.15)$$

Where  $\xi, \eta, \zeta$  are the natural coordinates shown in Figure 3.5. Equation (3.15) satisfies the two necessary conditions of the shape function:

- Condition of Nodal Compatibility

$$N_i(\xi_j, \eta_j, \zeta_j) = \begin{cases} 1 & \text{if } i = j \\ 0 & \text{if } i \neq j \end{cases} \quad (3.16)$$

- Rigid Body Condition:

$$\sum_{i=1}^n N_i(\xi, \eta, \zeta) = 1 \quad (3.17)$$

There is a specific bibliography regarding shapes functions and it can be reviewed in the corresponding bibliography [43, 20].

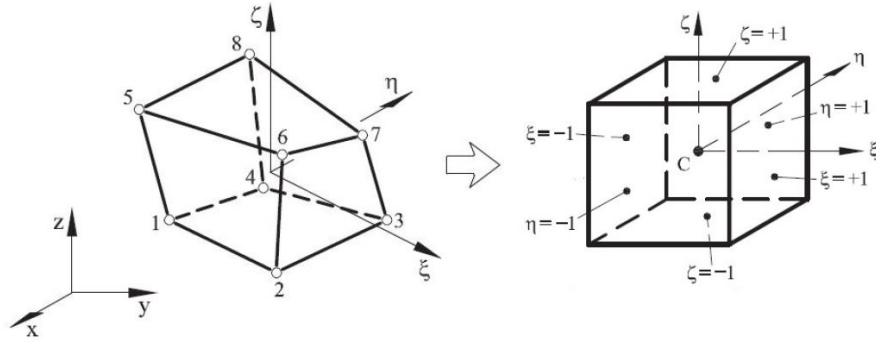


Figure 3.5: Example of a generic hexahedra FE and its normalized geometry [36].

### Discretization of the displacement field

As stated in reference [43], considering a 3D solid discretized into 8-noded hexahedras, the displacement field within each element can be expressed as:

$$u = \begin{Bmatrix} u \\ v \\ w \end{Bmatrix} = \sum_{i=1}^8 N_i a_i^{(e)} = N a^{(e)} \quad (3.18)$$

Where:

$$N = [N_1, N_2, \dots, N_8] N_i = \begin{bmatrix} N_i & 0 & 0 \\ 0 & N_i & 0 \\ 0 & 0 & N_i \end{bmatrix} \quad (3.19)$$

and

$$a^{(e)} = \begin{Bmatrix} a_1^{(e)} \\ a_2^{(e)} \\ \vdots \\ a_8^{(e)} \end{Bmatrix} a_i^{(e)} = \begin{Bmatrix} u_i \\ v_i \\ w_i \end{Bmatrix} \quad (3.20)$$

Are the shape function matrix and the displacement vector for each element and a node.

### Discretization of the strain field

The expression to describe the small strain field in terms of the FEM formulation is obtained by combining Equations (3.2) and (3.18). From which we get:

$$\varepsilon = \sum_{i=1}^8 \begin{Bmatrix} \frac{\partial N_i}{\partial x} u_i \\ \frac{\partial N_i}{\partial y} v_i \\ \frac{\partial N_i}{\partial z} w_i \\ \frac{\partial N_i}{\partial y} u_i + \frac{\partial N_i}{\partial x} v_i \\ \frac{\partial N_i}{\partial z} u_i + \frac{\partial N_i}{\partial x} w_i \\ \frac{\partial N_i}{\partial z} v_i + \frac{\partial N_i}{\partial y} w_i \end{Bmatrix} = \sum_{i=1}^8 \mathbf{B}_i a_i^{(e)} = \sum_{i=1}^8 \mathbf{B} a^{(e)} \quad (3.21)$$

Where  $\mathbf{B}$  is the deformation matrix of the element and  $\mathbf{B}_i$  is the deformation matrix of node  $i$ :

$$\mathbf{B} = [\mathbf{B}_1, \mathbf{B}_2, \dots, \mathbf{B}_8] \quad (3.22)$$

$$\mathbf{B}_i = \begin{bmatrix} \frac{\partial N_i}{\partial x} & 0 & 0 \\ 0 & \frac{\partial N_i}{\partial y} & 0 \\ 0 & 0 & \frac{\partial N_i}{\partial z} \\ \frac{\partial N_i}{\partial y} & \frac{\partial N_i}{\partial x} & 0 \\ \frac{\partial N_i}{\partial z} & 0 & \frac{\partial N_i}{\partial x} \\ 0 & \frac{\partial N_i}{\partial z} & \frac{\partial N_i}{\partial y} \end{bmatrix} \quad (3.23)$$

Obtaining the derivatives of shape functions with respect to Cartesian's coordinates requires the use of the chain rule.

### Equilibrium equation in FEM formulation

The PVW expression (Equation (3.14)) can be written using Equations (3.15) to (3.23). Where to get:

$$\iiint_V \mathbf{B}^T \sigma dV = \iiint_V \mathbf{N}^T \mathbf{b} dV + \iint_A \mathbf{N}^T \mathbf{t} dA + \Delta \mathbf{f}^{(e)} \quad (3.24)$$

This equation establishes the balance of internal and external forces in each element and it has been taken into account that the virtual deformation and virtual displacement are:

$$\delta \varepsilon = \mathbf{B} \delta \mathbf{a} \quad \delta \mathbf{u} = \mathbf{N} \delta \mathbf{a} \quad (3.25)$$

Analyzing each part of the Equation (3.24) we have that the left side of the equality is the internal nodal force vector for the element  $\mathbf{f}_{\text{int}}^{(e)}$  and the right side is the charge vector external, which gives the information of the forces applied to each element  $\mathbf{f}_{\text{ext}}^{(e)}$ . The expression is equivalent to:

$$\mathbf{f}_{\text{int}}^{(e)} - \mathbf{f}_{\text{ext}}^{(e)} = \Delta \mathbf{f}^{(e)} \quad (3.26)$$

This equation describes the vector of equilibrium nodal forces ( $\Delta \mathbf{f}^{(e)}$ ), that is, it has the information that guarantees the equilibrium of each element in the FEM formulation. Therefore, when the assembly is done, it only contains the information related to the reaction forces. This equation describes the vector of equilibrium nodal forces, that is, it has the information that guarantees the equilibrium of each element in the FEM. Therefore, when the assembly is done, it only contains the information related to the reaction forces [43].

Equation (3.24) can be rewritten as a system of equations considering the relationship between strain and stress given by Equation 3.6:

$$\begin{aligned} & \iiint_V \mathbf{B}^T \mathbf{C} \mathbf{B} dV \mathbf{a}^{(e)} - \iiint_V \mathbf{B}^T \mathbf{C} \varepsilon^0 dV + \\ & + \iiint_V \mathbf{B}^T \mathbf{C} \sigma^0 dV - \iiint_V \mathbf{N}^T \mathbf{b} dV - \iint_A \mathbf{N}^T \mathbf{t} dA = \Delta \mathbf{f}^{(e)} \end{aligned} \quad (3.27)$$

Using the concepts of stiffness matrix ( $\mathbf{K}^{(e)}$ ) and equivalent force vector ( $\mathbf{f}^{(e)}$ ) we can rewrite the Equation (3.27) in the equivalent form:

$$\mathbf{K}^{(e)} \mathbf{a}^{(e)} - \mathbf{f}^{(e)} = \Delta \mathbf{f}^{(e)} \quad (3.28)$$

Where:

Stiffness matrix :

$$\mathbf{K}^{(e)} = \iiint_V \mathbf{B}^T \mathbf{C} \mathbf{B} dV \quad (3.29)$$

Equivalent force vector :

$$\begin{aligned} \mathbf{f}^{(e)} = & \iiint_V \mathbf{B}^T \mathbf{C} \varepsilon^0 dV - \iiint_V \mathbf{B}^T \mathbf{C} \sigma^0 dV + \\ & + \iiint_V \mathbf{N}^T \mathbf{b} dV + \iint_A \mathbf{N}^T \mathbf{t} dA \end{aligned} \quad (3.30)$$

Equation (3.28) sets up the problem to be solved element by element with the contributions of  $\mathbf{K}^{(e)}$  and  $\mathbf{f}^{(e)}$  and thus form by assembling the global linear system of equations:

$$\mathbf{K} \mathbf{a} = \mathbf{f} \quad (3.31)$$

### 3.3 Solving the system of equations

This section shows the procedure to solve the proposed system of equations, which depends on whether the type of analysis is linear or nonlinear, to finally obtain the response of the model against the established boundary conditions.

When conduct a simulation of natural fibers in a composite material, the possibility of finding a nonlinear behavior is high, so the formulation for this thesis is carried out following to solve the nonlinear equation systems.

In this type of problem, the existence and uniqueness of the solution is not guaranteed. This makes it necessary to use a strategy that can reach equilibrium through the use of increments or continuity, which gives more information about the mechanical behavior of the system and also helps to trace the equilibrium path near the critical points and facilitates convergence.

There are several techniques that can be used to solve the system of equations, the options are the explicit or implicit methods. For this work an implicit approach has been used due to its robustness, stability and efficiency in static problems [35]. Using mechanisms with the Newton-Raphson technique and Arc-Length.

#### 3.3.1 Newton-Raphson Method

This iterative method assumes that, in a static analysis, the equilibrium equation has the general form:

$$\Delta \mathbf{f} = [\mathbf{f}^{int}(\mathbf{U})]^{t+\Delta t} - [\mathbf{f}^{ext}]^{t+\Delta t} = \mathbf{0} \quad (3.32)$$

Where  $f^{int}$  and  $f^{ext}$  are the internal and external force vectors.

Equation (3.32) is the objective function to solve, for this the algorithm will iterate until this established condition is reached. This expression can be written using the Taylor approximation series truncated in the second term:

$$\begin{aligned} 0 = {}^{i+1}[\Delta \mathbf{f}]^{t+\Delta t} &\simeq {}^i[\Delta \mathbf{f}]^{t+\Delta t} + {}^i \left[ \frac{\partial \Delta \mathbf{f}}{\partial \mathbf{U}} \right]^{t+\Delta t} {}^{i+1}[\Delta \mathbf{U}]^{n+1} = \\ &= {}^i[\Delta \mathbf{f}]^{t+\Delta t} + {}^i[\mathbf{J}]^{t+\Delta t} {}^i + 1[\Delta \mathbf{U}]^{t+\Delta t} \end{aligned} \quad (3.33)$$

Performing some mathematical operations such as using the inverse of the Jacobian, we obtain the Equation (3.34):

$${}^{i+1}[\Delta \mathbf{U}]^{t+\Delta t} = - ({}^i[\mathbf{J}]^{t+\Delta t})^{-1} {}^i[\Delta \mathbf{f}]^{t+\Delta t} \quad (3.34)$$

Finally, the displacement at the end of each iteration is written as:

$${}^{i+1}[\mathbf{U}]^{t+\Delta t} = {}^i[\mathbf{U}]^{t+\Delta t} + {}^{i+1}[\Delta\mathbf{U}]^{t+\Delta t} \quad (3.35)$$

Such that the displacement at the end of the linearized process, or it is also often said to converge, will be (see Figure 3.6).

It is a method that approximates the result in each calculation step, the convergence of this method is of second order, but there are some difficulties in its implementation which are described below [43, 35]:

- This method calculates the Jacobian matrix in each iteration, so the computational cost increases. There are other alternatives that modify this method to improve this problem, such as the modified Newton-Raphson, but this adjustment reduces the speed of convergence.
- There are cases where the Jacobian matrix is not symmetric and therefore its inversion is difficult (Antisymmetric Jacobian Operators).
- Another difficulty is that to achieve a second order convergence it is necessary to select a suitable point to start the iteration, that is, the speed of convergence depends on whether the point under study is close or far from the solution.
- When local extremums are encountered, the algorithm may lose information and have trouble finding the proper solution. This can be fixed by using helper techniques, such as displacement (Arc-Length) controlled methods.

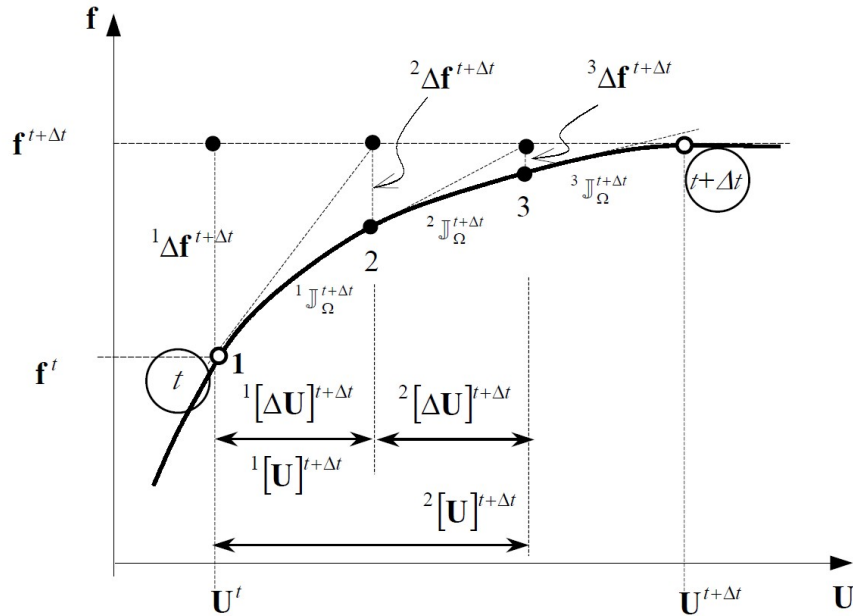


Figure 3.6: Newton-Raphson technique scheme 3.8.

### 3.3.2 Response control algorithms – “Arc-Length”

This method was used in this work due to the fact that in various structural mechanics problems states of unstable behavior can occur in which it is not possible to reach a coherent solution. To solve it or reduce the risk, a system of equilibrium equations with restrictions of the type  $\Delta \mathbf{f}(\ddot{\mathbf{U}}, \dot{\mathbf{U}}, \mathbf{U}, \lambda)$ , where the magnitude of the external force  $\lambda \mathbf{f}^{\text{ext}}$  is an unknown conditional on an additional equation  $c(\mathbf{U}, \lambda)$  [35]. Thus, a system of equilibrium equations amplified by this constraint equation is obtained:

$$\begin{cases} {}^{i+1}[\Delta \mathbf{f}(\ddot{\mathbf{U}}, \dot{\mathbf{U}}, \mathbf{U}, \lambda)]_{\Omega}^{k+\Delta t} = \mathbf{M}^{i+1}[\ddot{\mathbf{U}}]_{\Omega}^{+\Delta t} + {}^{i+1}[\mathbf{f}^{\text{int}}(\dot{\mathbf{U}}, \mathbf{U})]_{\Omega}^{++\Delta t} - {}^{i+1}[\lambda \mathbf{f}^{\text{ext}}]_{\Omega}^{+\Delta t} = \mathbf{0} \\ [c(\mathbf{U}, \lambda)]_{\Omega}^{l+\Delta t} = 0 \end{cases} \quad (3.36)$$

Developing the residual forces in Taylor series, in the neighborhood of the solution in time ( $t + \Delta t$ ), and considering that the velocity and acceleration parameters depend on the displacement field at this instant of time:

$$\begin{aligned} \Delta \mathbf{f}({}^i[\mathbf{U}] + {}^{i+1}[\delta \mathbf{U}], {}^i[\lambda] + {}^{i+1}[\delta \lambda]) = \mathbf{0} = \\ \Delta \mathbf{f}({}^i[\mathbf{U}], {}^i[\lambda]) + \left(\frac{\partial \Delta \mathbf{f}}{\partial \mathbf{U}}\right) {}^{i+1}[\delta \mathbf{U}]_{\Omega}^{t+\Delta t} + \left(\frac{\partial \Delta \mathbf{f}}{\partial \lambda}\right) {}^{i+1}[\delta \lambda] \end{aligned} \quad (3.37)$$

But in this last equation the following relations can be identified in Equation (3.33):

$$\left(\frac{\partial \Delta \mathbf{f}}{\partial \mathbf{U}}\right) = {}^i \mathbb{J} \quad ; \quad \left(\frac{\partial \Delta \mathbf{f}}{\partial \lambda}\right) = -\mathbf{f}^{\text{ext}} \quad (3.38)$$

That substituted in Equation (3.37), the system of equilibrium equations with restrictions is written in the form:

$$\begin{cases} \mathbf{0} = \Delta \mathbf{f}({}^i \mathbf{U}, {}^i \lambda) + {}^i \mathbb{J} \cdot {}^{i+1}[\delta \mathbf{U}] - \mathbf{f}^{\text{ext}} \cdot {}^{i+1}[\delta \lambda] \\ 0 = {}^{i+1}[c(\mathbf{U}, \lambda)] \end{cases} \quad (3.39)$$

With this we obtain the field of displacements:

$$\begin{aligned} {}^i \mathbb{J} \cdot {}^{i+1}[\delta \mathbf{U}] &= -\Delta \mathbf{f}({}^i \mathbf{U}, {}^i \lambda) + \mathbf{f}^{\text{ext}} \cdot {}^{i+1}[\delta \lambda] \\ {}^i \mathbb{J}^{i+1}[\delta \mathbf{U}] &= - \underbrace{\left[ \mathbf{M}^i[\ddot{\mathbf{U}}] + {}^i[\mathbf{f}^{\text{int}}(\dot{\mathbf{U}}, \mathbf{U})] \cdot {}^i[\lambda \mathbf{f}^{\text{ext}}] \right]}_{{}^i \mathbb{J} \cdot {}^{i+1}[\delta \dot{\mathbf{U}}]} + {}^i \mathbb{J}^{i+1}[\mathbf{U}]_{\text{TOT}} \cdot {}^{i+1}[\delta \lambda] \end{aligned} \quad (3.40)$$

Since the Jacobian operator is the same on both sides of the above equation, we can write the displacement increment as:

$${}^{i+1}[\delta\mathbf{U}]^{i+1}[\delta\hat{\mathbf{U}}] + {}^{i+1}[\mathbf{U}]_{\text{TOT}} {}^{i+1}[\delta\lambda] \quad (3.41)$$

We obtain:

$$\begin{cases} {}^i\mathbb{J}^{i+1}[\delta\hat{\mathbf{U}}] = - \left[ \mathbb{M}^i[\mathbf{U}] + {}^i[\mathbf{f}^{\text{int}}(\mathbf{U}, \mathbf{U})]^i [\lambda \mathbf{f}^{\text{ext}}] \right] \\ {}^i\mathbb{J} \cdot {}^{i+1}[\mathbf{U}]_{\text{TOT}} = \mathbf{f}^{\text{ext}} \\ {}^{i+1}[\lambda] = [\lambda] + {}^{i+1}[\delta\lambda] \end{cases} \quad (3.42)$$

Where  ${}^{i+1}[\mathbf{U}]_{\text{TOT}}$  is the total displacement obtained with the last, or maximum, external force value,  ${}^{i+1}[\delta\hat{\mathbf{U}}]$  is the solution of the system of equations without correction and  $\delta^{i+1}\lambda$  is the change in the load application factor.

Once the general equations of the method have been defined, it is necessary to specify the form of the restriction equation, in this work one of the most common was used, which is called "Spherical Control Equation". It is based on requiring that a certain displacement increment norm be contained within a hyper-Sphere in the displacement space [35]:

$${}^{i+1}[c(\mathbf{U}, \lambda)]^{i+1}[\Delta\mathbf{U}]^T \cdot {}^{i+1}[\Delta\mathbf{U}] - \Delta\ell^2 = 0 \quad (3.43)$$

Where the displacement and its increment is obtained as:

$${}^{i+1}[\mathbf{U}]^{t+\Delta t} = {}^1[\mathbf{U}]^t + {}^{i+1}[\Delta\mathbf{U}]^{t+\Delta t} \quad ; \quad {}^{i+1}[\Delta\mathbf{U}]^{t+\Delta t} = {}^i[\Delta\mathbf{U}]^{t+\Delta t} + {}^{i+1}[\delta\mathbf{U}]^{t+\Delta t} \quad (3.44)$$

Substituting Equation 3.41 in 3.44 and the resulting equation in 3.3.2, we will obtain the control equation written in time  $t + \Delta t$ :

$$\begin{aligned} \left\{ {}^i[\Delta\mathbf{U}] + {}^{i+1}[\delta\hat{\mathbf{U}}] + {}^{i+1}[\mathbf{U}] \quad {}^{i+1}[\delta\lambda] \right\}^T \cdot \left\{ {}^i[\Delta\mathbf{U}] + {}^{i+1}[\delta\hat{\mathbf{U}}] + {}^{i+1}[\mathbf{U}]_{\text{TOT}} \quad {}^{i+1}[\delta\lambda] \right\} - \Delta\ell^2 = 0 \\ \Downarrow \\ C_1^{i+1}[\delta\lambda]^2 + C_2^{i+1}[\delta\lambda] + C_3 = 0 \end{aligned} \quad (3.45)$$

Where the coefficients of this second degree equation are the following:

$$\begin{aligned} C_1 &= {}^{i+1}[\mathbf{U}]_{\text{TOT}}^T \quad {}^{i+1}[\mathbf{U}]_{\text{TOT}} \\ C_2 &= 2 \left[ {}^i[\Delta\mathbf{U}] + {}^{i+1}[\delta\hat{\mathbf{U}}] \right]^T \cdot {}^{i+1}[\mathbf{U}]_{\text{TOT}} \\ C_3 &= \left[ {}^i[\Delta\mathbf{U}] + {}^{i+1}[\delta\hat{\mathbf{U}}] \right]^T \cdot \left[ {}^i[\Delta\mathbf{U}] + {}^{i+1}[\delta\hat{\mathbf{U}}] \right] - \Delta\ell^2 \end{aligned} \quad (3.46)$$

As reference [35] suggests, all that remains is to solve the quadratic equation in  ${}^{i+1}[\delta\lambda]$  and the load factor correction is obtained (see Figure 3.7):

$${}^{i+1}[\delta\lambda] = -\frac{C_2}{2C_1} \pm \frac{(C_2^2 - 4C_1C_3)^{1/2}}{2C_1} \Rightarrow \begin{cases} {}^{i+1}[\delta\lambda]_1 \\ {}^{i+1}[\delta\lambda]_2 \end{cases} \quad (3.47)$$

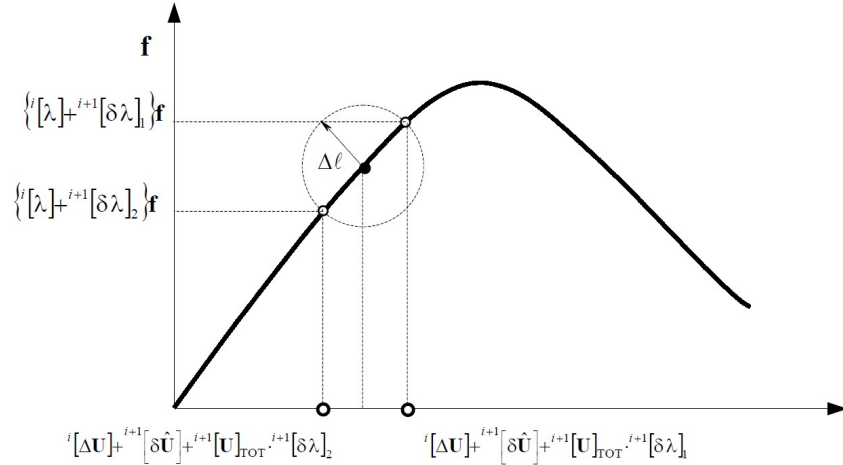


Figure 3.7: “Arc-Length” spherical path – Detail of the solution search [35].

Once the two possible load factors  ${}^{i+1}[\delta\lambda]_{1,2}$  have been obtained, it is necessary to determine which of them is correct. For this, it explores about the correct forward direction,  ${}^{i+1}[\delta\mathbf{U}]{}^{i+1}[\delta\hat{\mathbf{U}}] + {}^{i+1}[\mathbf{U}]_{\text{TOT}}{}^{i+1}[\delta\lambda]_{1,2}$ , which is assumed to be is the one whose angle with the displacement increment in the previous step  ${}^i[\Delta\mathbf{U}]$  is maximum [35] (Figure 3.8).

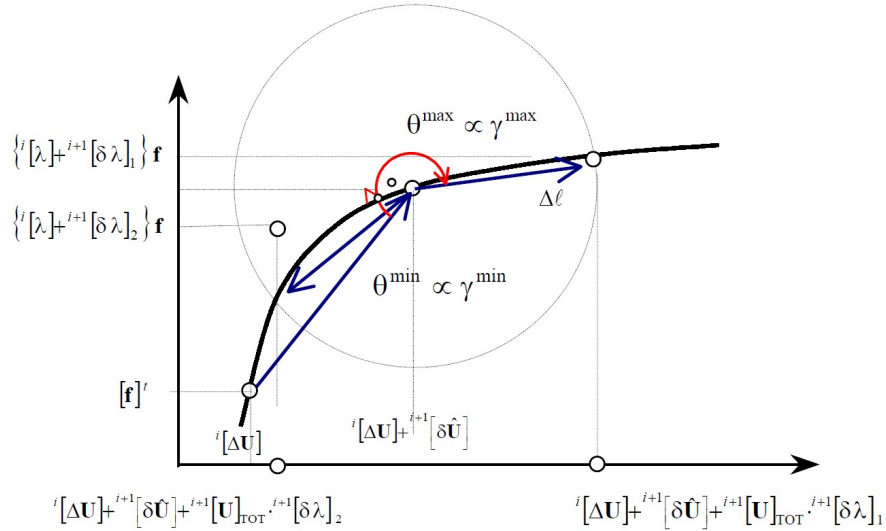


Figure 3.8: “Arc-Length” spherical path – Progress detail in the solution [35].

This address results from the following scalar product:

$$\begin{aligned}\gamma^1 &= {}^{i+1}[\Delta\mathbf{U}]_1^T \cdot {}^i[\Delta\mathbf{U}] \\ \gamma^2 &= {}^{i+1}[\Delta\mathbf{U}]_2^T \cdot {}^i[\Delta\mathbf{U}]\end{aligned}\tag{3.48}$$

Such that the  ${}^{i+1}[\delta\lambda]_{1,2}$  is chosen which gives rise to the  ${}^{i+1}[\Delta\mathbf{U}]_{1,2}$  which makes maximum  $\gamma_j$ .

# Chapter 4

## Serial-Parallel Rule of Mixtures (SP-RoM)

As we know, the study of composite materials is related to the scale in which we are evaluating the material and therefore this characteristic is extremely important when choosing the types of models or existing techniques to simulate composite materials. Having micromechanical, macromechanical or homogenization methodologies.

### 4.1 Serial-Parallel Rule of Mixtures Theory

As commented at the beginning of this section, this specific theory consists of homogenizing the response or phenomena of the composite material based on the individual behavior of each component, with the incorporation of new fundamentals that allow overcoming the limitation of the parallel mixing theory. and considering the direction as an important aspect in the behavior of the compound.

This theory incorporates a combination of iso-strain conditions and iso-stress conditions that achieve a more realistic and accurate simulation of the composite material. The fundamentals of SP-RoM are based on the parallel mixing principle with the difference that the iso-strain is considered as [35]:

- All components are subjected to the same strain field in a certain specific direction, usually the direction in which the fibers are oriented (parallel direction).

In addition to introducing a new foundation related to the iso-tension:

- All components are subjected to the same stress field in the remaining directions, iso-stress condition. (serial direction).

## 4.2 Formulation of Serial-Parallel Rule of Mixtures Theory

The formulation shown in this section is applicable to small deformations and will show mathematically how the properties of the components are combined in the mechanical calculation of the composite material.

The first step is to note that the SP-RoM is an MDF and for this reason the strain and stress are calculated from the average value of the field of each one:

$$\bar{\varepsilon} := \frac{\int_{\Omega} \varepsilon dV}{\int_{\Omega} dV} \quad \bar{\sigma} := \frac{\int_{\Omega} \sigma dV}{\int_{\Omega} dV} \quad (4.1)$$

Where  $\Omega \subset \mathbb{R}$  is the reference frame of the composite material.

### Compatibility conditions of the formulation

The compatibility conditions [43, 53] are the starting point for the development of the SP RoM theory and its respective functioning. These are derived from the compatibility conditions required in the CMT (Mixing Theory) and defined by the authors Trusdell and Toupin [48]. These are necessary to build the formulation that allows coupling the constitutive behavior of N simple materials modeled with any constitutive law. The compatibility conditions are:

- Each infinitesimal volume of composite material contains a finite number of component materials.
- Each component volume is significantly lower than the composite volume.
- The contribution of each component to the composite global behaviour is proportional to their volumetric participation in the infinitesimal volume.
- All the component materials are perfectly bonded (no relative displacement).
- All the component materials are subjected to the same strain field in a specific direction (parallel direction).
- All the component materials are subjected to the same stress field in a specific direction (serial direction).

### SP-RoM problem description

When defining the serial and parallel directions that control the behavior of the composite, it is important to determine which composite material is being modeled, as it was already described, in the first section of this document, that there are different types of composite materials where one of those types It is reinforced with long fibers.

In this type of composites, the direction that determines the parallel behavior is equivalent to the direction of the fibers. In a real structure modeled using the FEM, it is imposed element by element. In mathematical terms, the parallel direction is defined using the vector  $e_1$  that is oriented along the material fiber [13].

$$\mathbf{N}_P = \mathbf{e}_1 \otimes \mathbf{e}_1 \quad (4.2)$$

Where  $e_1$  is the basis vector that locally defines the parallel behavior in the element and  $\mathbf{N}_P$  is the second order parallel projection tensor, which is used to obtain the projection in the direction of the fiber of a vector  $v$ :

$$v_P = \mathbf{N}_P v \quad (4.3)$$

As detailed by the author Sergio J. [43], the frame of reference is completed with the base vectors  $e_2$  and  $e_3$  that define the serial behavior. It is important to note that for this case the parallel behavior is imposed only in one direction, that is,  $e_1$ . This only occurs in long-fiber composites, but can be extended to two dimensions (sheet materials) or all three (full parallel behavior, i.e. CMT approach) or switch to full series behavior.

Using the tensor  $\mathbf{N}_P$  we can calculate the parallel and serial components of strain and stress. This is done defining the fourth order parallel projector  $\mathbb{P}_P$ :

$$\mathbb{P}_P = \mathbf{N}_P \otimes \mathbf{N}_P \quad (4.4)$$

The fourth order serial projector  $\mathbb{P}_S$  :

$$\mathbb{P}_S = \mathbb{I} - \mathbb{P}_P \quad (4.5)$$

It is possible to define the parallel and serial components of the strain and stress fields (Equation (4.6)) as:

$$\begin{aligned} \varepsilon_P &= \mathbb{P}_P : \varepsilon & \varepsilon_S &= \mathbb{P}_S : \varepsilon \\ \sigma_P &= \mathbb{P}_P : \sigma & \sigma_S &= \mathbb{P}_S : \sigma \end{aligned} \quad (4.6)$$

Now, we can obtain a description of the fourth-order constitutive tensor  $\mathbb{C}$  using the above decompositions of the stress and strain fields:

$$\begin{bmatrix} \sigma_P \\ \sigma_S \end{bmatrix} = \begin{bmatrix} \mathbb{C}_{PP} & \mathbb{C}_{PS} \\ \mathbb{C}_{SP} & \mathbb{C}_{SS} \end{bmatrix} : \begin{bmatrix} \varepsilon_P \\ \varepsilon_S \end{bmatrix} \quad (4.7)$$

Where:

$$\begin{aligned} \mathbb{C}_{PP} &= \mathbb{P}_P : \mathbb{C} : \mathbb{P}_P = \frac{\partial \sigma_P}{\partial \varepsilon_P} & \mathbb{C}_{PS} &= \mathbb{P}_P : \mathbb{C} : \mathbb{P}_S = \frac{\partial \sigma_P}{\partial \varepsilon_S} \\ \mathbb{C}_{SP} &= \mathbb{P}_S : \mathbb{C} : \mathbb{P}_P = \frac{\partial \sigma_S}{\partial \varepsilon_P} & \mathbb{C}_{SS} &= \mathbb{P}_S : \mathbb{C} : \mathbb{P}_S = \frac{\partial \sigma_S}{\partial \varepsilon_S} \end{aligned} \quad (4.8)$$

Finally, Equation (4.5) shows that the parallel and series decompositions are complementary. This can be extended to the field of strains and stresses.

$$\begin{aligned} \varepsilon &= \varepsilon_P + \varepsilon_S \\ \sigma &= \sigma_P + \sigma_S \end{aligned} \quad (4.9)$$

### Matrix and fibre relations in composite materials

The general equations presented above are necessary in the SP RoM to describe the behavior at all scales in the material, this means that they are used to describe the behavior of the entire composite material, but also the components of the matrix and the fiber [43].

Using the compatibility conditions written above, the following expressions can be derived for a composite material with only two components: fibre and matrix.

Specifically, Equation (4.10) mathematically represents compatibility condition 2 of the model, in a similar way Equations (4.11) and (4.12) are the expressions of compatibility conditions 5 and 6.

$$\varepsilon = {}^f k^f \varepsilon + {}^m k^m \varepsilon \quad \sigma = {}^f k^f \sigma + {}^m k^m \sigma \quad (4.10)$$

$$\text{Parallel direction : } \begin{cases} c_{\varepsilon_P} = {}^f \varepsilon_P = {}^m \varepsilon_P \\ c_{\sigma_P} = {}^f k^f \sigma_P + {}^m k^m \sigma_P \end{cases} \quad (4.11)$$

$$\text{Serial direction : } \begin{cases} c_{\varepsilon_S} = {}^f k^f \varepsilon_S + {}^m k^m \varepsilon_S \\ c_{\sigma_S} = {}^f \sigma_S = {}^m \sigma_S \end{cases} \quad (4.12)$$

Considering that in Equation (4.10), index (c) corresponds to the composite, (f) to the fiber and (m) to the matrix, in addition to the fact that  $^f k$  and  $^m k$  are coefficients that reflect the volumetric contribution of each component and therefore verify the condition  $^f k + ^m k = 1$ . It is important to keep in mind that the condition 2 is still prevailing. Thus:

$$^c \varepsilon_P = ^f k ^f \varepsilon_P + ^m k ^m \varepsilon_P = ^c \varepsilon_P (^f k + ^m k) = ^c \varepsilon_P \quad (4.13)$$

$$^c \sigma_S = ^f k ^f \sigma_S + ^m k ^m \sigma_S = ^c \sigma_S (^f k + ^m k) = ^c \sigma_S \quad (4.14)$$

### Closure equations of the constitutive model of the composite

The SP RoM formulation is controlled by the strain field, which is the independent driving variable [43, 42, 45]. For this reason, the current state at a point  $x_i$  in any of the component materials that constitute a fiber and matrix composite is completely defined with the strain field at the studied point i.e.  $^f \varepsilon(x_1)$  and  $^m \varepsilon(x_2)$ , where  $x_1 \subset \Omega_f, x_2 \subset \Omega_m$  and  $\Omega = \Omega_f \cup \Omega_m$  and also by a finite set of internal variables denoted by the vector  $^f \boldsymbol{\beta}$  for fiber and  $\theta_u$  for matrix.

This relationship is expressed as:

$$^f S = \{^f \varepsilon, ^f \boldsymbol{\beta}\} \quad ^m S = \{^m \varepsilon, ^m \boldsymbol{\beta}\} \quad (4.15)$$

Just as Sergio J. [43] explains, for the composite material the problem is governed by the Cartesian product of the two sets  $^f S$  and  $^m S$  and the composite mean strain ( $^c \varepsilon$ ):

$$I = ^f S \times ^m S = \{^f \varepsilon, ^m \varepsilon, ^f \boldsymbol{\beta}, ^m \boldsymbol{\beta}\} \quad (4.16)$$

At this point in the formulation of the SP RoM, it has been possible to propose a mathematical description of the relationship between the components of the composite material, but the system of equations that allows the study of the composite element has not yet been completed. The missing equations are those that describe the interaction between the materials that make up the compound, that is, the closing equations:

$$f_i = (^f \varepsilon, ^m \varepsilon, ^f \boldsymbol{\beta}, ^m \boldsymbol{\beta}, ^f \boldsymbol{\sigma}, ^m \boldsymbol{\sigma}) = 0, \quad i = 1, \dots, 6 \quad (4.17)$$

An example described by references [43, 42] of an appropriate closure equation for long fiber composites (LFC) is the one used in the Serial-Parallel Basic model (SPB model). This equation is independent of the internal variables of each component  $^f \boldsymbol{\beta}$  and  $^m \boldsymbol{\beta}$  and can be written as:

$$^f \varepsilon_P = ^m \varepsilon_P \quad ^f \sigma_S = ^m \sigma_S \quad (4.18)$$

As explained, there are other closure equations that can be used instead, but the simplicity of this one has made it widely used for the analysis of composite materials. Despite this, it is important to be aware of the limitations of this approach, produced by the isostrain condition in the serial direction leading to inaccurate predictions of transverse stiffness.

Finally the system of equations that controls the composite behavior is completed [42, 45]:

$$\left\{ \begin{array}{l} {}^f \dot{\boldsymbol{\sigma}} = {}^f g({}^f \boldsymbol{\varepsilon}, {}^f \boldsymbol{\beta}, {}^f \dot{\boldsymbol{\varepsilon}}) \\ {}^f \dot{\boldsymbol{\beta}} = {}^f h({}^f \boldsymbol{\varepsilon}, {}^f \boldsymbol{\beta}, {}^f \dot{\boldsymbol{\varepsilon}}) \\ {}^m \dot{\boldsymbol{\sigma}} = {}^m g({}^m \boldsymbol{\varepsilon}, {}^m \boldsymbol{\beta}, {}^m \dot{\boldsymbol{\varepsilon}}) \\ {}^m \dot{\boldsymbol{\beta}} = {}^m h({}^m \boldsymbol{\varepsilon}, {}^m \boldsymbol{\beta}, {}^m \dot{\boldsymbol{\varepsilon}}) \\ \boldsymbol{\varepsilon} = {}^f k^f \boldsymbol{\varepsilon} + {}^m k^m \boldsymbol{\varepsilon} \\ \boldsymbol{\sigma} = {}^f k^f \boldsymbol{\sigma} + {}^m k^m \boldsymbol{\sigma} \\ {}^f \varepsilon_P = {}^m \varepsilon_P \\ {}^f \sigma_S = {}^m \sigma_S \end{array} \right. \quad (4.19)$$

Where the first four expressions of Equation (4.19) correspond to the constitutive models of the component materials. These describe the stress and the evolution of the internal variables in terms of the independent variables (Equation 4.15).

### Algorithm for the solution of the SP-RoM problem

We know the driving variables that define the problem (Equation (4.16)) and the set of equations that govern it (Equation (4.19)). The statement of the problem can be formulated, as the authors explain [43, 42], in the following way knowing the driving variables at time  $t$ :

$${}^t [{}^f \boldsymbol{\varepsilon}], {}^t [{}^m \boldsymbol{\varepsilon}], {}^t [{}^f \boldsymbol{\beta}], {}^t [{}^m \boldsymbol{\beta}], {}^t [\boldsymbol{\varepsilon}] \quad (4.20)$$

And the composite material strain at time  $t + \Delta t$ :

$${}^{t+\Delta t} [\boldsymbol{\varepsilon}] \quad (4.21)$$

Find out the updated state for composite at time  $t + \Delta t$ , defined by the variables:

$${}^{t+\Delta t} [{}^f \boldsymbol{\varepsilon}], {}^{t+\Delta t} [{}^m \boldsymbol{\varepsilon}], {}^{t+\Delta t} [{}^f \boldsymbol{\beta}], {}^{t+\Delta t} [{}^m \boldsymbol{\beta}], {}^{t+\Delta t} [{}^f \boldsymbol{\sigma}], {}^{t+\Delta t} [{}^m \boldsymbol{\sigma}], {}^{t+\Delta t} [\boldsymbol{\sigma}] \quad (4.22)$$

Which satisfy the equations that control the compound behavior in the time interval  $t + \Delta t$ .

The independent variable to be chosen for the Newton-Raphson algorithm is the serial component of the deformation matrix ( ${}^m\varepsilon_S$ ) and the residual to minimize is the unbalance of serial voltages ( $\Delta\sigma_S$ ), defined as:

$$\Delta\sigma_S = {}^m\sigma_S - {}^f\sigma_S \quad (4.23)$$

Only one independent variable is needed for the approach, the other variables of the problem, for both component materials, can be calculated from an initial approximation of  ${}^m\varepsilon_S$ .

The steps that must be followed to solve the problem posed above are presented below (Figure 4.1). If these steps are included in an FE code as a composite constitutive model [43, 42], the code will be adequate for modeling the problem.

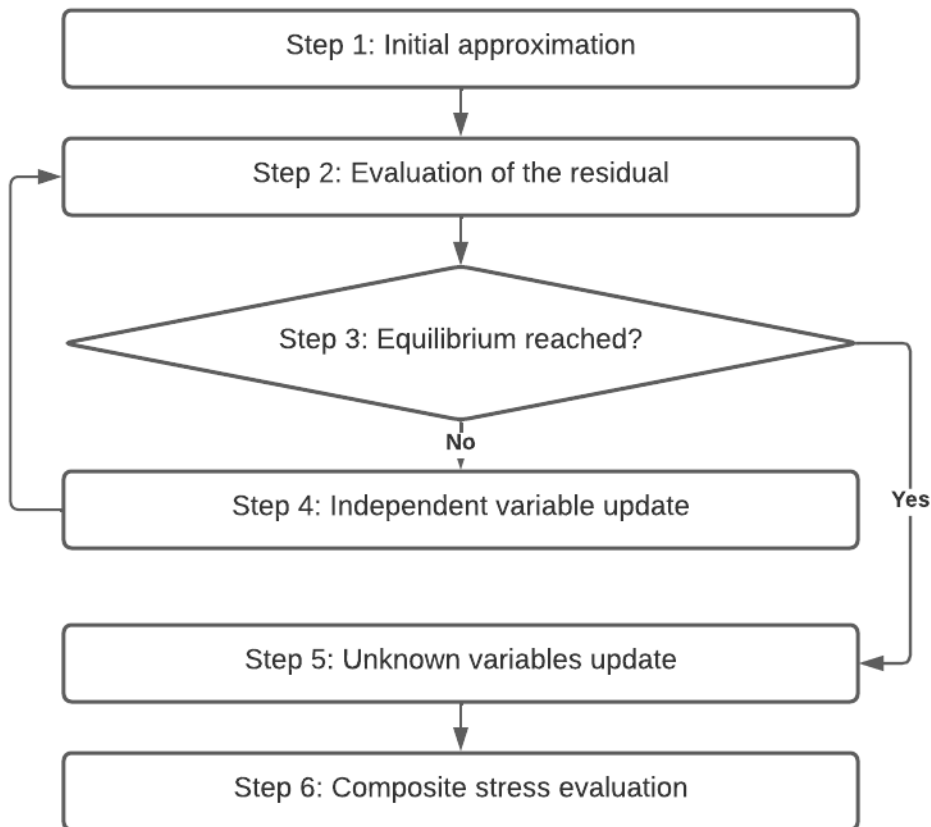


Figure 4.1: Flowchart with the strategy to solve the proposed system of equations.

**Step 1 - Initial approximation:**

In every iterative process an initial value is needed for the variable  ${}^m\varepsilon_S$ . The precision of this initial approximation is fundamental for the number of iterations necessary for the convergence of the problem. For this reason, it is important to provide a good value for the first iteration,  $[{}^m\varepsilon_S]_{k=0}$ . This is generally achieved by considering linear behavior for all component materials. If the hypothesis is true, the value obtained will be correct and no iterations will be needed. This is expressed as:

$$[{}^m\Delta\sigma]_0 = {}^t[{}^m\mathbf{C}] : [{}^m\Delta\varepsilon]_0 \quad (4.24)$$

$$[{}^f\Delta\sigma]_0 = {}^t[{}^f\mathbf{C}] : [{}^f\Delta\varepsilon]_0 \quad (4.25)$$

Where  $[{}^i\Delta\bullet]_0 = {}^{t+\Delta t}[{}^i\bullet]_0 - {}^t[{}^i\bullet]$  with  $i = f$  or  $m$  is the increment of the variable  $[{}^i\bullet]$  from one step to the next, the subscript 0 indicates the first iteration of the new step  $t + \Delta t$  and  ${}^t[{}^i\mathbf{C}]$  is the tangent constitutive tensor of each component material  $i = f$  or  $m$ , computed using the set of known variables shown in Equation (4.20).

Considering now only the serial terms of the previous expressions, as set in Equation (4.7):

$$[{}^m\Delta\sigma_S]_0 = {}^t[{}^m\mathbf{C}_{SS}] : [{}^m\Delta\varepsilon_S]_0 + {}^t[{}^m\mathbf{C}_{SP}] : [{}^m\Delta\varepsilon_P]_0 \quad (4.26)$$

$$[{}^f\Delta\sigma_S]_0 = {}^t[{}^f\mathbf{C}_{SS}] : [{}^f\Delta\varepsilon_S]_0 + {}^t[{}^f\mathbf{C}_{SP}] : [{}^f\Delta\varepsilon_P]_0 \quad (4.27)$$

Using this equation and the closing condition described in (4.18) we obtain:

$$\begin{aligned} \overbrace{[{}^m\Delta\sigma_S]_0 - [{}^f\Delta\sigma_S]_0}^{=0} &= {}^t[{}^m\mathbf{C}_{SS}] : [{}^m\Delta\varepsilon_S]_0 + {}^t[{}^m\mathbf{C}_{SP}] : \overbrace{[{}^m\Delta\varepsilon_P]_0}^{=[\Delta\varepsilon_P]_0} - \\ &\quad - {}^t[{}^f\mathbf{C}_{SS}] : [{}^f\Delta\varepsilon_S]_0 + {}^t[{}^f\mathbf{C}_{SP}] : \overbrace{[{}^f\Delta\varepsilon_P]_0} \\ \implies 0 &= {}^t[{}^m\mathbf{C}_{SS}] : [{}^m\Delta\varepsilon_S]_0 - {}^t[{}^f\mathbf{C}_{SS}] : [{}^f\Delta\varepsilon_S]_0 + \\ &\quad + ({}^t[{}^m\mathbf{C}_{SP}] - {}^t[{}^f\mathbf{C}_{SP}]) : [\Delta\varepsilon_P]_0 \end{aligned} \quad (4.28)$$

This equation can be simplified using the Compatibility Conditions of serial direction in Equation (4.12):

$$\begin{aligned} 0 &= {}^t[{}^m\mathbf{C}_{SS}] : [{}^m\Delta\varepsilon_S]_0 - {}^t[{}^f\mathbf{C}_{SS}] : \left( \frac{1}{f_k} [\Delta\varepsilon_S]_0 - \frac{m_k}{f_k} [{}^m\Delta\varepsilon_S]_0 \right) + \\ &\quad + ({}^t[{}^m\mathbf{C}_{SP}] - {}^t[{}^f\mathbf{C}_{SP}]) : [\Delta\varepsilon_P]_0 \implies \\ \implies \left( {}^t[{}^m\mathbf{C}_{SS}] + \frac{m}{f} {}^t[{}^f\mathbf{C}_{SS}] \right) &: [{}^m\Delta\varepsilon_S]_0 = \\ = \frac{1}{f_k} {}^t[{}^f\mathbf{C}_{SS}] : [\Delta\varepsilon_S]_0 &+ ({}^t[{}^m\mathbf{C}_{SP}] - {}^t[{}^f\mathbf{C}_{SP}]) : [\Delta\varepsilon_P]_0 \end{aligned} \quad (4.29)$$

And finally, setting:  $\mathbb{A} = ({}^f k^t [{}^m \mathbb{C}_{SS}] + {}^m k^t [{}^f \mathbb{C}_{SS}])^{-1}$ , Equation (4.29) is rewritten as:

$$[{}^m \Delta \varepsilon_S]_0 = \mathbb{A} : [{}^t [{}^f \mathbb{C}_{SS}] : [\Delta \varepsilon_S]_0 + {}^f k ({}^t [{}^m \mathbb{C}_{SP}] - {}^t [{}^f \mathbb{C}_{SP}]) : [\Delta \varepsilon_P]_0] \quad (4.30)$$

From this equation,  ${}^{t+\Delta t} [{}^m \varepsilon_S]_{k=0}$  is computed ( ${}^{t+\Delta t} [{}^m \varepsilon_S]_{k=0} = {}^t [{}^m \varepsilon_S] + [{}^m \Delta \varepsilon_S]_0$ ) and the algorithm moves to step 2.

### Step 2 - Evaluation of the residual:

As commented in reference [43], Once the independent variable  ${}^{t+\Delta t} [{}^m \varepsilon_S]_k$  has been obtained, it is necessary to determine its reliability by means of the residual. It is computed as shown in Equation (4.23), using the serial stress values at  $t + \Delta t$  of each component material. Thus, obtaining  ${}^{t+\Delta t} [{}^m \sigma]$  and  ${}^{t+\Delta t} [{}^f \sigma]$  is the main objective of this step because Equation (4.6) allows the computation of the serial component of these variables.

The first thing to do before the serial stress imbalance could be estimated, is to determine the total strains for each component:

$$\begin{aligned} [{}^m \varepsilon]_k &= [{}^m \varepsilon_P] + [{}^m \varepsilon_S]_k, \text{ where: } [{}^m \varepsilon_P] = [{}^f \varepsilon_P] = [\varepsilon_P] \\ [{}^f \varepsilon_k]_k &= [{}^f \varepsilon_P] + [{}^f \varepsilon_S]_k, \text{ where: } [{}^f \varepsilon_S]_k = \frac{1}{f_k} [\varepsilon_S] - \frac{{}^m k}{f_k} [{}^m \varepsilon_S]_k \end{aligned} \quad (4.31)$$

These equations are based on the complementary property of the serial and parallel parts of the strain and stress fields and are valid for all the iterations of the problem, therefore,  $k$  is not necessary equal to 0.

Finally, the stresses and the internal variables are computed based on the real constitutive model of each component material (the elastic hypothesis used at step 1 is no longer valid) and the residual  $\Delta \sigma_S = {}^m \sigma_S - {}^f \sigma_S$  is evaluated.

### Step 3 - Equilibrium reached:

The algorithm is able to decide if the solution obtained for the set of variables in step  $t + \Delta t$  is adequate or not. This decision is made in relation to the tolerance indicated. Its value is imposed based on the serial efforts of each component in the previous step  $t$ , i.e.  $\text{tol} \sim f ({}^t [{}^i \sigma_S])$ , where  $i = f, m$ . This function is defined as:

$$\begin{aligned} f_1 ({}^t [{}^m \sigma_S], {}^t [{}^f \sigma_S]) &= \min \{ \| \| {}^t [{}^m \sigma_S] \|, \| {}^t [{}^f \sigma_S] \| \} \\ f_2 ({}^t [{}^m \sigma_S], {}^t [{}^f \sigma_S]) &= \min \{ \| \| {}^t [{}^m \mathbb{C}_{SS}] : [\varepsilon_S] \|, \| {}^t [{}^f \mathbb{C}_{SS}] : [\varepsilon_S] \| \} \end{aligned} \quad (4.32)$$

$$\text{tol} = 10^{-4} \cdot \begin{cases} f_1 ({}^t [{}^m \sigma_S], {}^t [{}^f \sigma_S]), & \text{if } f_1 ({}^t [{}^m \sigma_S], {}^t [{}^f \sigma_S]) > 0 \\ f_2 ({}^t [{}^m \sigma_S], {}^t [{}^f \sigma_S]), & \text{if } f_1 ({}^t [{}^m \sigma_S], {}^t [{}^f \sigma_S]) = 0 \end{cases}$$

Therefore:

If  $\|[\Delta\sigma_S]_k\| \leq \text{tol}$  then go to Step 5.  
 If  $\|[\Delta\sigma_S]_k\| > \text{tol}$  then go to Step 4.

**Step 4 - Independent variable update:**

If this step must be performed from the previous state, it is because  ${}^{t+\Delta t} [{}^m \varepsilon_S]_k$  value is not good enough according to the tolerance computed at step 3. In this case,  ${}^{t+\Delta t} [{}^m \varepsilon_S]_k$  should be recalculated as follows :

- a) Compute the tangent constitutive tensor for each component material  ${}^{t+\Delta t} [{}^i \mathbf{C}]_k$  using the results of the current iteration step k, i.e.  ${}^{t+\Delta t} [{}^i \varepsilon]_k$  and  ${}^{t+\Delta t} [{}^i \boldsymbol{\beta}]_k$ .
- b) Jacobian matrix computation [42]:

$${}^{t+\Delta t} [\mathbb{J}]_k = {}^{t+\Delta t} [{}^m \mathbf{C}_{SS}]_k + {}^m k t + \Delta t [{}^f \mathbf{C}_{SS}]_k \quad (4.33)$$

Where  $[{}^m \mathbf{C}_{SS}]$  and  $[{}^f \mathbf{C}_{SS}]$  are computed as shown in Equation (4.8) from the tangent constitutive tensors  $[{}^m \mathbf{C}]$  and  $[{}^f \mathbf{C}]$ . This expression is obtained from the general Jacobian definition and using its notation:  $\Delta f = \Delta \sigma_S$  and  $u = {}^m \varepsilon_S$ . Therefore:

$$\begin{aligned} [\mathbb{J}]_k &= \left. \frac{\partial [\Delta \sigma_S]}{\partial {}^m \varepsilon_S} \right|_{m {}^m \varepsilon_S = [{}^m \varepsilon_S]_k} = \frac{\partial [{}^m \sigma_S]_k}{\partial {}^m \varepsilon_S} - \frac{\partial [{}^f \sigma_S]_k}{\partial {}^f \varepsilon_S} : \frac{\partial {}^f \varepsilon_S}{\partial {}^m \varepsilon_S} = \\ &= [{}^m \mathbf{C}_{SS}]_k - [{}^f \mathbf{C}_{SS}]_k : \left( -\frac{{}^m k}{f_k} \mathbb{I} \right) = \\ &= \underbrace{[{}^m \mathbf{C}_{SS}]_k + \frac{{}^m k}{f_k} [{}^f \mathbf{C}_{SS}]_k}_{\text{Eq.4.33}} \end{aligned} \quad (4.34)$$

- c) Unknown  ${}^{t+\Delta t} [{}^m \varepsilon_S]_k$  update:

$${}^{t+\Delta t} [{}^m \varepsilon_S]_{k+1} = {}^{t+\Delta t} [{}^m \varepsilon_S]_k - {}^{t+\Delta t} [\mathbb{J}]_k^{-1} : [\Delta \sigma_S]_k \quad (4.35)$$

Once this has been done, the algorithm moves back to step 2 and starts a new iteration  $k + 1$ .

### Step 5 - Unknown variables update:

Once the problem has converged, it is necessary to prepare the data for the next time step. The results of the variables indicated in the equation are now the known variables of the new time step.

### Step 6 - Composite stress evaluation:

Finally the composite total stress is computed ( ${}^{t+\Delta t}[\boldsymbol{\sigma}]$ ):

$${}^{t+\Delta t}[\boldsymbol{\sigma}] = {}^f k^{t+\Delta t} [{}^f \boldsymbol{\sigma}] + {}^m k^{t+\Delta t} [{}^m \boldsymbol{\sigma}] \quad (4.36)$$

As Sergio explains in reference [43], this algorithm is used to obtain the unknowns at all the composite elements of the FE mesh used in the simulation. This provides the local solution of the problem, but the global behaviour is still unknown. The global solution for the structure is obtained through the Equation (3.31), where the global stiffness matrix is made up of all the composite tangent constitutive tensors  $\mathbb{C}$  from each element of the FE mesh. Two approaches can be followed in order to obtain these tensors:

- Calculation using numerical perturbations [35]. At this stage, the stress and strain fields of the composite material are known, therefore the composite  $\mathbb{C}$  tensor can be obtained activating small strains and analysing the results obtained, i.e.  $\mathbb{C} = \boldsymbol{\sigma} : \boldsymbol{\varepsilon}^{-1}$
- Calculation through the component tangent constitutive tensors [42, 45]. The composite tangent constitutive tensor has been defined in Equations (4.6) and (4.7). These expressions can be written in terms of the components tangent constitutive tensors as:

$$\begin{aligned} \mathbb{C}_{PP} &= {}^m k {}^f k ({}^f \mathbb{C}_{PS} - {}^m \mathbb{C}_{PS}) : \mathbb{A} : ({}^f \mathbb{C}_{SP} - {}^m \mathbb{C}_{SP}) + \\ &\quad + ({}^f k {}^f \mathbb{C}_{PP} + {}^m k {}^m \mathbb{C}_{PP}) \\ \mathbb{C}_{PS} &= ({}^f k {}^f \mathbb{C}_{PS} : \mathbb{A} : {}^m \mathbb{C}_{SS} + {}^m k {}^m \mathbb{C}_{PS} : \mathbb{A} : {}^f \mathbb{C}_{SS}) \\ \mathbb{C}_{SP} &= ({}^m k {}^f \mathbb{C}_{SS} : \mathbb{A} : {}^m \mathbb{C}_{SP} + {}^f k {}^m \mathbb{C}_{SS} : \mathbb{A} : {}^f \mathbb{C}_{SP}) \\ \mathbb{C}_{SS} &= \frac{1}{2} [({}^m \mathbb{C}_{SS} : \mathbb{A} : {}^f \mathbb{C}_{SS}) + ({}^f \mathbb{C}_{SS} : \mathbb{A} : {}^m \mathbb{C}_{SS})] \end{aligned} \quad (4.37)$$

By doing this, it is possible now to solve the global system of equations and move to the next time step.



# Chapter 5

## Numerical Characterization of Organic Composite Materials

For more than two decades, the reinforcement of composite materials using organic fibers has taken on significant relevance due to their ability to replace glass reinforcements that are widely used in today's industry. Natural fibers such as banana, jowar, coconut, sisal and jute have attracted the attention of scientists and engineers for applications in consumer goods, low-cost housing, automotive components, among others.

Natural fibers have many advantages compared to synthetic fibers, such as low density, cheaper and acceptable specific properties, and they are also renewable and biodegradable [7]. They also have high resistance and rigidity, good thermal and acoustic insulating properties and high resistance to fracture. However, one of the difficulties when working with this type of reinforcement is the lack of validation when it comes to numerical models and also certainty in their material properties, generating doubts in engineers when using these materials for their designs.

In this section, two specimens of composite materials with organic fiber reinforcement will be studied, which were tested in compression and tension tests to determine their mechanical behavior. Using the SP-RoM theory and the Kratos Multiphysics [37, 12] with GiD calculation tool, a nonlinear numerical approximation of the composite materials is developed, which are compared with the experimental results found in the bibliography.

A complex calibration work has been carried out, due to the little information available regarding organic composite materials. In addition to the fact that there are not numerous numerical studies of these compounds and the behavior of the studied theory should be explored. The calibration of the properties is complex due to the high non-linearity of these materials, added to the difficulty of obtaining a high certainty of the mechanical properties of organic elements experimentally. This is due to the fact that many factors can produce variability in the experimental results, such as the quality of the natural product, humidity, manufacturing method, etc. For this reason, being able to obtain a curve that approximates the experimental results involves an arduous and methodical iterative process.

## 5.1 Numerical characterization of polyester resin specimen reinforced with jowar fiber

The aim of this section is to describe the mechanical and numerical characterization of this organic compound material was carried out, beginning with the procedure that Prasad et al [7] used to make the test specimens for his study, where his results are the basis for the numerical characterization carried out.

### 5.1.1 Experimental tension test

The experimental study of the mechanical properties was carried out by the reference [7], where an unsaturated polyethylene resin matrix was used with properties of 1258 kg/m<sup>3</sup> of density and 500 cps of viscosity at 25 °C and 35% of content in monomer. This matrix is reinforced with natural jowar fibers. The author mentions that the fiber manufacturing method contemplates that these fibers are collected by cutting the stem of the plant, then the leaves are removed from the nodes and the tips of the canes are trimmed. After trimming the culms are dried in the shade for a period of one week. The node portions are removed by cutting and the culms are separated into pieces of the required length. These cylindrical pieces that contain lignin in the central part are converted into strips by peeling them in the longitudinal direction and the lignin is removed, which is very soft in the case of jowar. These strips were kept in water for a period of about 3 h to soften them and were subjected to a mechanical process by gently hitting them with a plastic mallet to loosen and separate the fiber. The resulting fiber bundle is discarded and combed down to individual fibers.

Material	Density (Kg/m <sup>3</sup> )	Tensile strength (MPa)	Tensile modulus (GPa)
Polyethylene Resin	1150	31.5	0.63
Jowar Fibers	922	302	6.99
Composite 40% Fiber	1056	124	2.75

Table 5.1: Mechanical properties of composite materials [7].

Prasad et al [7] used the manual lamination method to fill the prepared mold with a suitable amount of polyester resin mixture and layers of unidirectional continuous jowar fibers, so that it begins and ends with resin layers. The amount of accelerator and catalyst added to the resin at room temperature for curing was 1.5% by volume of resin each. Fiber strain and movement must be minimized to produce good quality unidirectional fiber composites. Therefore, at the time of curing a compression pressure of 0.05 MPa was applied on the mold and the composite samples were cured for 24 h. Specimens were also post-cured at 70 C for 2 h after removal from the mold.

The specimens that were built in this study are tested for tensile tests. The author emphasizes that 160 mm fibers are used for tensile tests and considers that the fibers are equivalent to 40% of the total volume of the composite .

The unidirectional composite specimens were made as per the ASTM D 638-89 [6] to measure the tensile properties. The length, width and thickness of the specimens were 160, 12.5 and 3 mm, respectively.

The author [7] worked five identical samples that were prepared for each volume fraction of fibre. Although all the specimens were tested at a strain rate of 0.5 mm/min using an electronic tensometer, we will only consider the 40% fiber of volume fraction . The density of the fibre and its composites were measured using picnometric procedure.

### 5.1.2 Results of the numerical characterization

Based on the properties of the constituent materials of the composite and using the SP RoM theory, the base properties of the composite material are calculated to begin with the numerical characterization. Considering that the volumetric fraction of the fiber in the composite is 40%, we obtain (See Equation (5.1)):

$$E_C = E_F V_F + E_M V_M \quad (5.1)$$

Being  $E_C$  the properties of the compound,  $E_F$  the properties of the fiber and  $E_M$  the properties of the matrix, in the same way  $V_F$  and  $V_M$  are the volumetric fractions of the fiber and the matrix respectively.

Material	Fiber [F]	Matrix [M]	Composite [C]
Tensile strength (MPa)	302	31.5	140
Young modulus (GPa)	6.99	0.63	3.17

Table 5.2: Calculated mechanical properties of component materials.

Subsequently, the geometric model of the specimen described above was carried out considering a symmetry in the X and Y axis, that is, a quarter of the specimen is considered in order to be able to reduce the number of elements of the model and thus have a lower computational expense. This geometry was meshed with first order hexahedral structured elements of size 1 mm. The geometry and the mesh can be seen in Figure 5.1 :

As seen in Figure 5.1, 3 boundary conditions are considered for this model, group 1 of brown color being the one corresponding to symmetry with respect to the X axis, group 2 of yellow color is the condition of symmetry with respect to the Y axis and finally group 3 in gray is a condition of constant displacement in each time step of the model. This allows the tensile test to be established numerically.

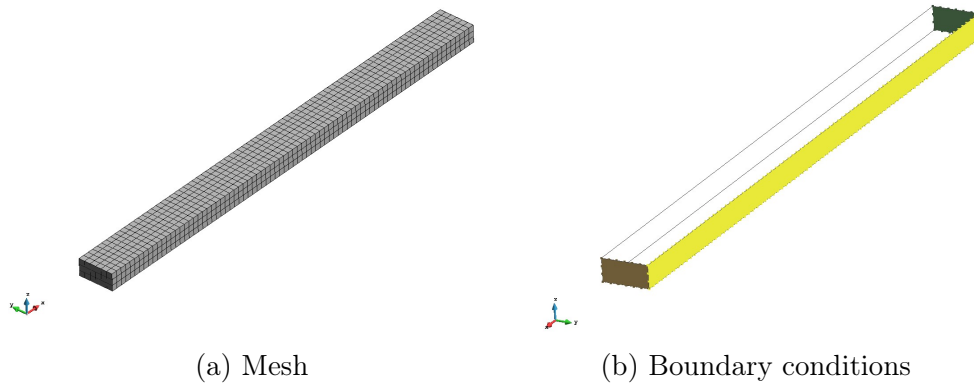


Figure 5.1: Specimen with dimensions 6.25x3x80 mm with a mesh of 2,268 nodes.

Based on the experimental results of the reference [7], the static numerical model is calibrated considering that the matrix and the fibers follow the theories of small deformations, isotropic behavior with an orientation of fibers in the X axis and considering damage model in the fiber and matrix of the composite (see Figure 5.2). This calibration is performed with an iterative process where the properties of the material and the fracture energy are adjusted in order to obtain a result that represents those obtained experimentally by the author [7].

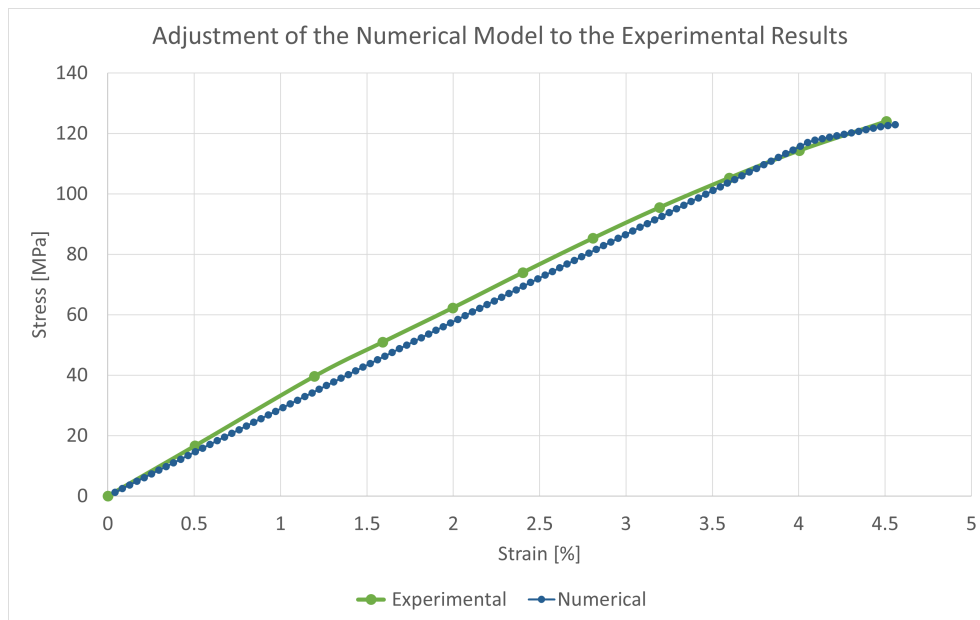


Figure 5.2: Results of the numerical model calibrating the composite material.

The final configuration of the component materials is shown in the following Table 5.3, these values differ from those obtained in the theoretical calculation of Equation (5.1), although the percentage is not greater than 1 %. This may be due to the large number of factors that can modify the properties of organic fiber.

Material	Fiber [F]	Matrix [M]	Composite [C]
Tensile strength (MPa)	255	33.0	122
Young modulus (GPa)	6.30	0.61	2.89

Table 5.3: Calibrated mechanical properties of calculated component materials.

This simulation established a time step of 0.01 s to achieve an optimal convergence of the results, in addition, two different flow rules were employed for the matrix and the fiber, in the case of the matrix an Exponential Hardening approach was established and for the fiber of Initial Hardening Exponential Softening. The selection of these flow rules was studying the behavior of the material during the iterative calibration process.

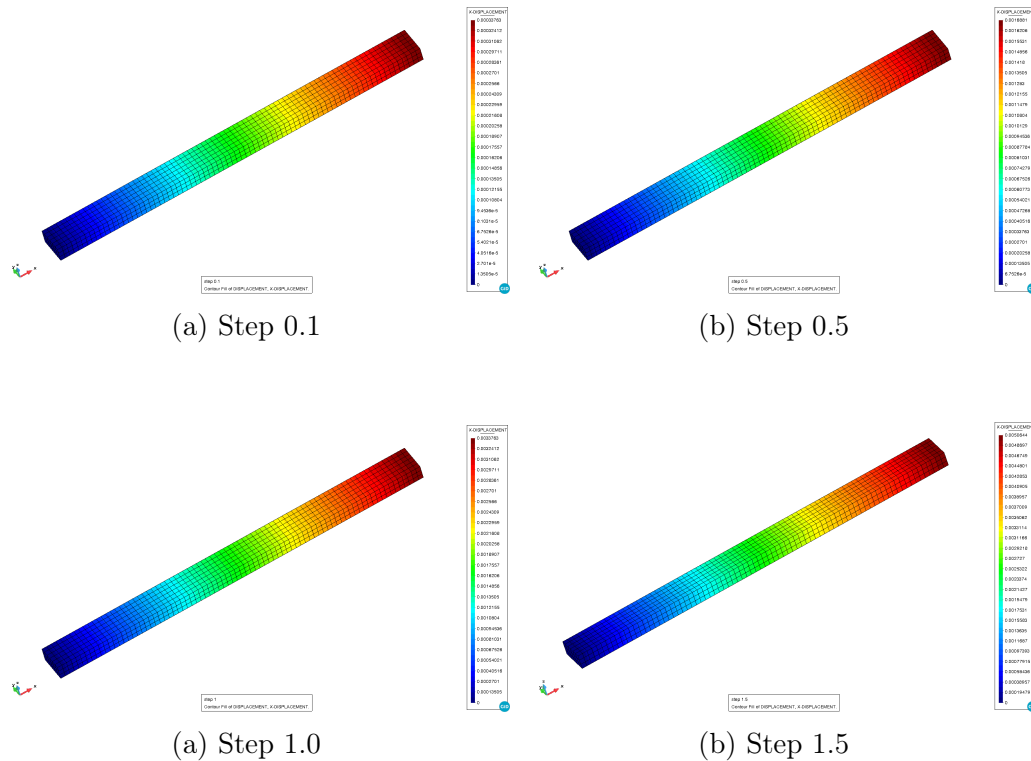


Figure 5.4: X-axis displacements for different steps of the numerical model.

Once the materials have been properly calibrated, a numerical simulation of a 3-point bending test is carried out, to study the mechanical response of the numerical characterization carried out with the composite material. The results obtained from the simulation are compared with a theoretical calculation of bending to verify that the composite material has been correctly characterized.

### 5.1.3 Theoretical and numerical characterization of bending test

In the same way of the chapter 5.1.2, we built a geometry of the characteristics that can be seen in Figure 5.5, this geometry was meshed with first order hexahedral structured elements of size 0.5 mm. In addition, planes of symmetry are established for the X and Y axis (Figure 5.5).

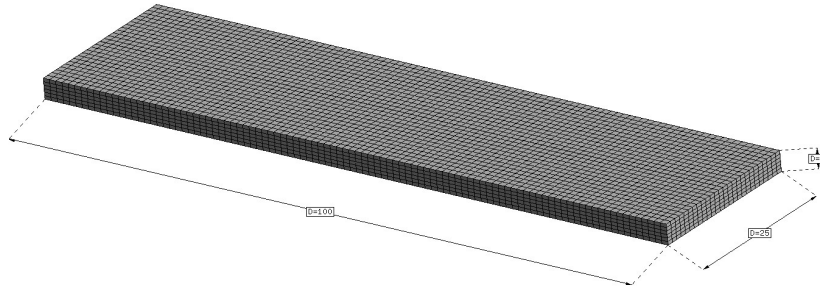


Figure 5.5: First order hexahedral structured mesh with 19,089 nodes.

Using the same mechanical properties of the material components in the calibration of the numerical tensile model and with a variable time step from 0.1 to 0.001 s, we obtain the following results.

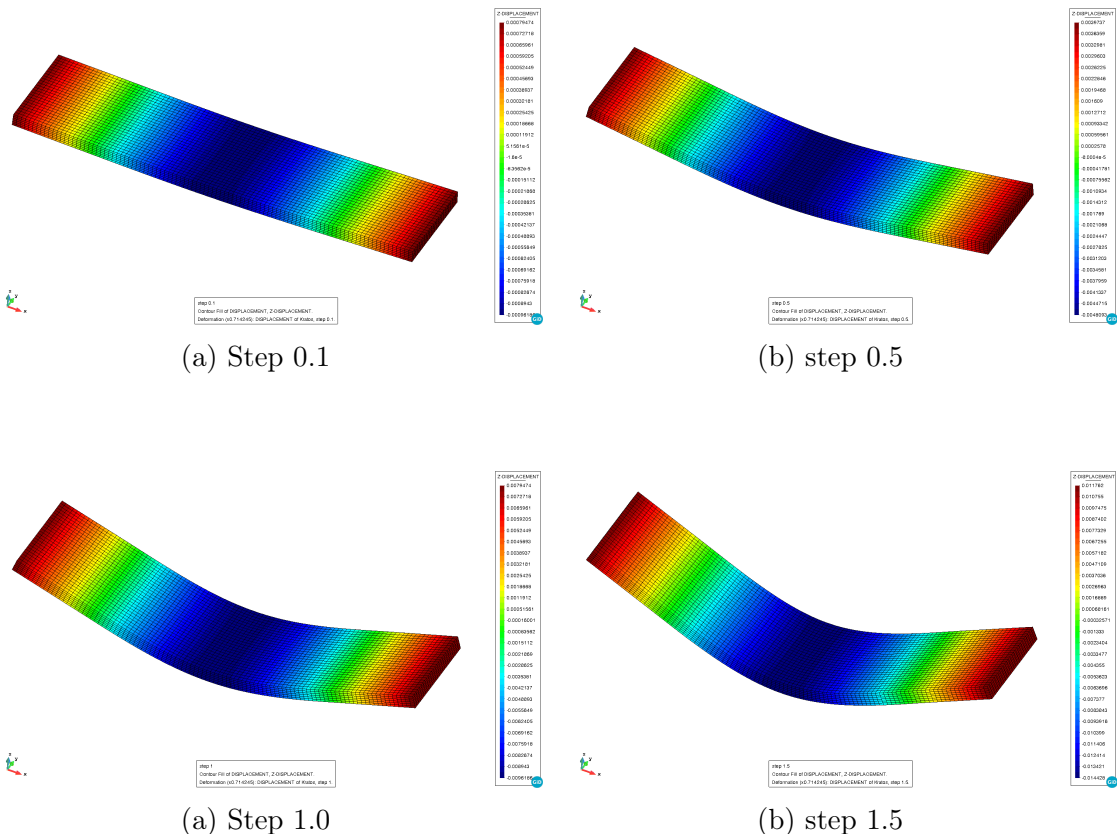


Figure 5.7: Results of bending in Z axis of the numerical model in different steps.

To validate that these results are representative, a theoretical calculation of the bending of this specimen is made, for this a comparison is used in a Force-Displacement graph at the midpoint of the specimen.

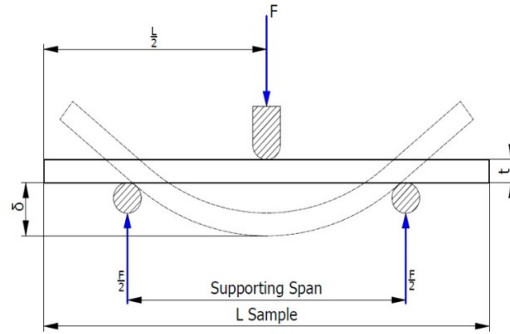


Figure 5.8: Scheme and variables of the 3-point bending test.

Using the Equation (5.2), which considers the inertia of a rectangle, we obtain the force to carry out the comparison, we can see that the behavior with the results of the numerical model are equivalent until the moment of fracture, where the Nonlinear behavior of the compound cannot be approximated by theory.

$$\delta = \frac{F \cdot L^3}{48 \cdot E \cdot I} \quad (5.2)$$

Being F: the applied force, L: the separation of the specimen between the support points, E: the modulus of elasticity of the material and I: the inertia of the specimen considering a rectangular section. The comparison of theoretical and numerical results are presented in Figure 5.9:

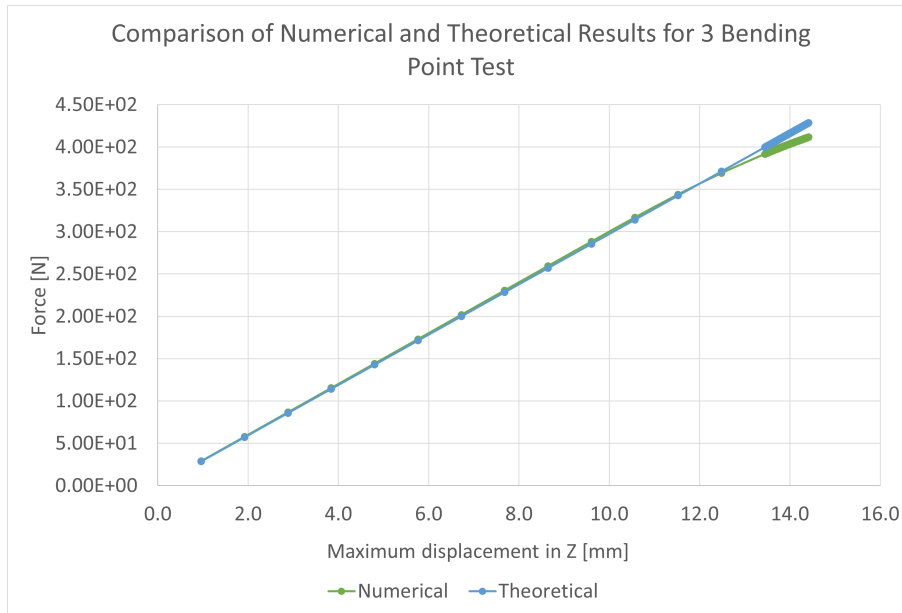


Figure 5.9: Validation of the numerical model with calibrated materials.

### 5.1.4 Analysis of results

The use of the SP RoM theory has been successful in numerically characterizing the mechanical behavior of the polyester resin compound reinforced with Jowar fiber, although the calibration of the component materials was not easy, the numerical model manages to represent the elastic and plastic behavior of the material composite with long oriented fiber. In the calibration stage, the key factor has been the use of an initial hardening exponential softening flow rule for the fiber, since this, added to the iterative process of fracture energy calibration, achieves the maximum effort documented by the author in his experimental tests with a non-linear behavior generated by the damage of the fibers.

In Figure 5.2 one can see that the linear behavior of the material has a difference of 5% in young's modulus and less than 1% in the maximum stress, the greatest difference is in the modulus of young and may be due to the fact that the behavior of the compound changes to non-linear after a percentage of 1% of the Strain, where the experienced material begins to deform with a changing slope until it breaks. This short linearity may be due to the fact that the matrix is being damaged in the areas close to the fibers, while the latter bear the tensile load, keeping the curve from reducing its slope abruptly. This behavior is common in composite materials because one of the failure modes is related to the adhesion between the reinforcing fiber and the matrix.

The numerical model cannot approximate this fiber-matrix interaction, because the theoretical approach of SP RoM simplifies the material to a homogeneous one as explained above, but despite this, the behavior and mechanical properties of the composite are validated with the bending model theoretical Figure 5.9. In this model, the maximum deflection recorded in the numerical model was compared with the expected theoretical behavior.

It can be seen that the numerical model fits the young's modulus that characterizes the slope of the curve and that the maximum force is reached, only with the difference that the numerical model manages to obtain the non-linear behavior of the material due to the flow rule used in the fiber, while the theoretical cannot represent this nonlinear behavior.

## 5.2 Numerical characterization of Foamed Concrete specimen reinforced with Henequen fiber

In the same way as the previous section, we proceed to describe the mechanical characterization of this composite reinforced with disperse organic fiber, explaining the procedure obtained by the author J. Castillo [41], where compression and tension tests were carried out on experimental specimens. The information of this reference is used for the numerical characterization of the material.

### 5.2.1 Composite material characteristics

J.Castillo [41] explains that cell concrete is a type of cement in which air bubbles are trapped in the mortar. The density of this type of concrete can vary between 400 and 1600 kg/m<sup>3</sup> [24]. One of the characteristics of cellular concrete is that it has good workability and is classified as lightweight concrete. It can be used in filling applications, thermal insulation, acoustic insulation, fire resistance and impact energy absorption applications; however, foam concrete is not often used as a structural material due to its low compressive strength. Also, foam concrete is not good at supporting tensile loads.

The content design of the cellular concrete mixture used in this investigation is shown in Table 5.4, which is known as simple cellular concrete (PFC). The mixture was prepared with Portland cement, limestone aggregate, water and foam. Portland cement CPC 30R EXTRA (Cemex, Mérida, México) with a minimum strength of 30 MPa at 28 days was used. [11].

Constituent	Content [Kg]
Cement	342
Limestone aggregate	171
Water	240
Foam	29

Table 5.4: The mixture that was prepared with Portland cement [41].

The fibers of the reinforcement are of natural origin extracted from the henequen plant (*Agave fourcroydes* Lem.), as the author comments [41], the henequen fibers were supplied by local producers in Baca, Yucatan (Desfibradora La Lupita, Baca, Mexico). Henequen fibers were cut to a length of 19 mm. For the fiber-reinforced treated mixtures, henequen fibers were treated with a 2% (w/v; ie, 2.04 g NaOH per 100 mL solution) aqueous solution of sodium hydroxide (NaOH) for 1 hour. at 25°C. using a mechanical stirrer at 550 rpm. Subsequently, the fibers were washed with water until all sodium hydroxide was removed. Finally, the fibers were dried in an oven at 60 °C for 24 h [49].

Foamed concrete with a target dry density of 700 kg/m<sup>3</sup> was prepared using the prefoaming method [41], which consists of 3 stages: (1) preparation of the liquid cement mixture (mortar); (2) preparation of the foam and (3) mixing of the mortar and foam. The materials were mixed until a homogeneous mixture was obtained. The foam was prepared separately using a JFG200 foam generator and EABASSOC foaming agent (EAB Associates, Altrincham, UK). As the author explains, a mixture of the foaming agent and water (31 mL of foaming agent per liter of water) was used to prepare the foam. This mixture was then poured into the foam generator container. The container was pressurized to 0.689 MPa (100 psi), which produced a foam density of  $50 \pm 2.5$  kg/m<sup>3</sup>. Finally, the foam was poured into the mixer containing the mortar until reaching a wet density of 800 kg/m<sup>3</sup>.

Finally, the properties of the foamed concrete and the treated fibers are:

Material	Density (Kg/m <sup>3</sup> )	Tensile strength (MPa)	Tensile modulus (GPa)
Foamed Concrete	700	3.0	1.2
Henequen Fibers	1400	1.0	0.13

Table 5.5: Mechanical properties of component materials [41].

### 5.2.2 Experimental compression and tension tests.

J.Castillo [41] evaluated the compressive behavior of the specimen in accordance with BS EN 12390 using a Shimadzu AG-1 universal testing machine, equipped with a 100 kN load cell, and a crosshead speed of 2.4 mm/min. It is noted that the compressive displacement of the samples was measured using the crosshead displacement of the universal testing machine and, consequently, the precision in the measurement of the elastic deformations is limited. Cubic specimens with dimensions of 100 mm x 100 mm x 100 mm were used. Specimens were cured in molds for 1 day after casting; then, they were unmolded and cured in a plastic bag for 24 days. Subsequently, the specimens were removed from the bag and air-cured for 3 days at a temperature of 25 °C. All samples were analyzed 28 days after casting.

The specimens tested in compression and tension can be seen in Figure 5.10.

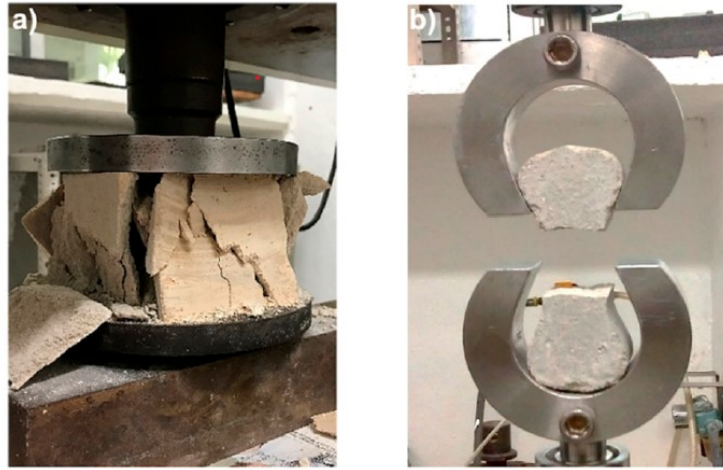


Figure 5.10: (PFC) specimens: (a) compression test and (b) tension test [41].

Castillo [41] also performed uniaxial tensile tests using briquette samples (dog-bone shaped samples Figure 5.11 with a length of 76 mm and a cross-sectional area of 25.4 mm x 25.4 mm in the central section. All samples were analyzed 28 days after casting. He also used a Shimadzu AG-1 universal testing machine with a 20 kN load cell. The load was applied at a constant displacement speed of 1 mm/min.

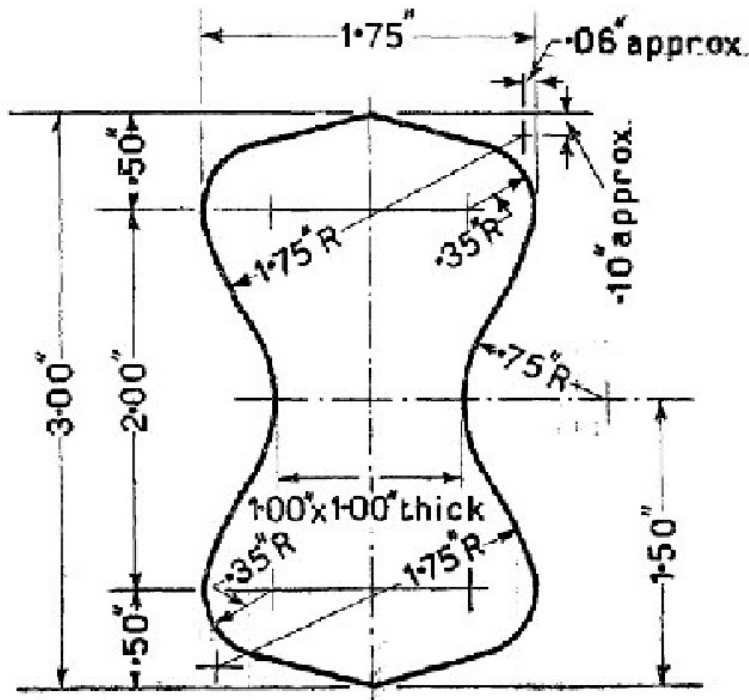


Figure 5.11: Briquette samples (dog-bone shape).

### 5.2.3 Results of the numerical characterization of compression

Based on the properties of the constituent materials of the composite and applying the Parallel RoM theory, since we are dealing with a mixture of dispersed fibers, and considering a damage model for fiber and matrix. The base properties of the composite material are calculated to begin with the numerical characterization. Considering that the volumetric fraction of the compound studied is 50% for each component, we obtain (see Equation (5.1)):

Material	Fiber [F]	Matrix [M]	Composite [C]
Tensile strength (MPa)	1.00	3.00	2.00
Young modulus (GPa)	0.13	1.20	0.67

Table 5.6: Calculated mechanical properties of component materials.

Subsequently, the calibration of the numerical model began considering the experimental data of the compression test, for this the rectangular specimen described by the author is built, taking into account symmetries in the 3 axes, this means that an eighth of a specimen with their respective symmetries being their dimensions 50 x 50 x 50 mm, this can be seen in Figure 5.12:

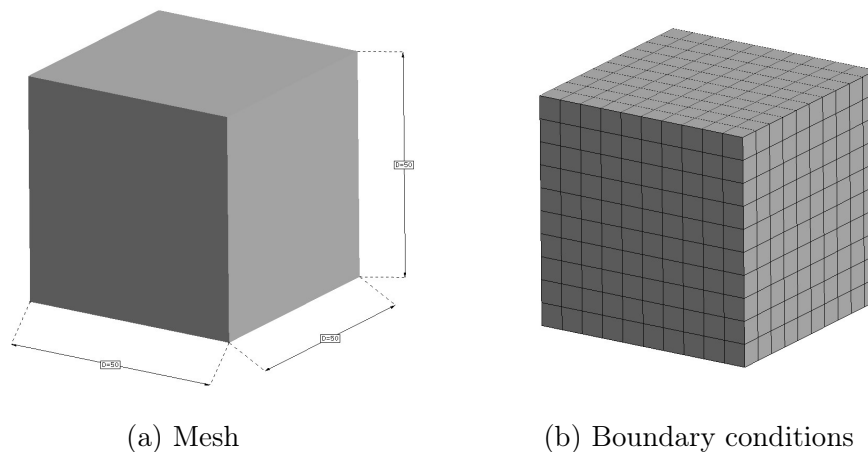


Figure 5.12: 5 mm hexahedral structured mesh with 1331 nodes.

Based on the experimental results of the reference [41], the numerical model is calibrated considering that the matrix and the fibers follow the theories of small deformations, isotropic behavior with a dispersed fiber orientation and considering a softening model for fiber and for concrete a modified Mohr Coulomb damage approach [35]. This calibration is carried out with an iterative process where the properties of the material and the fracture energy are adjusted in order to obtain a result that represents those obtained experimentally by the author Castillo [41].

Both materials have an exponential hardening flow rule which gave good results to adjust the behavior of the compound. The compression load was also applied with a time step of 0.1 s. The results can be seen in Figure 5.14:

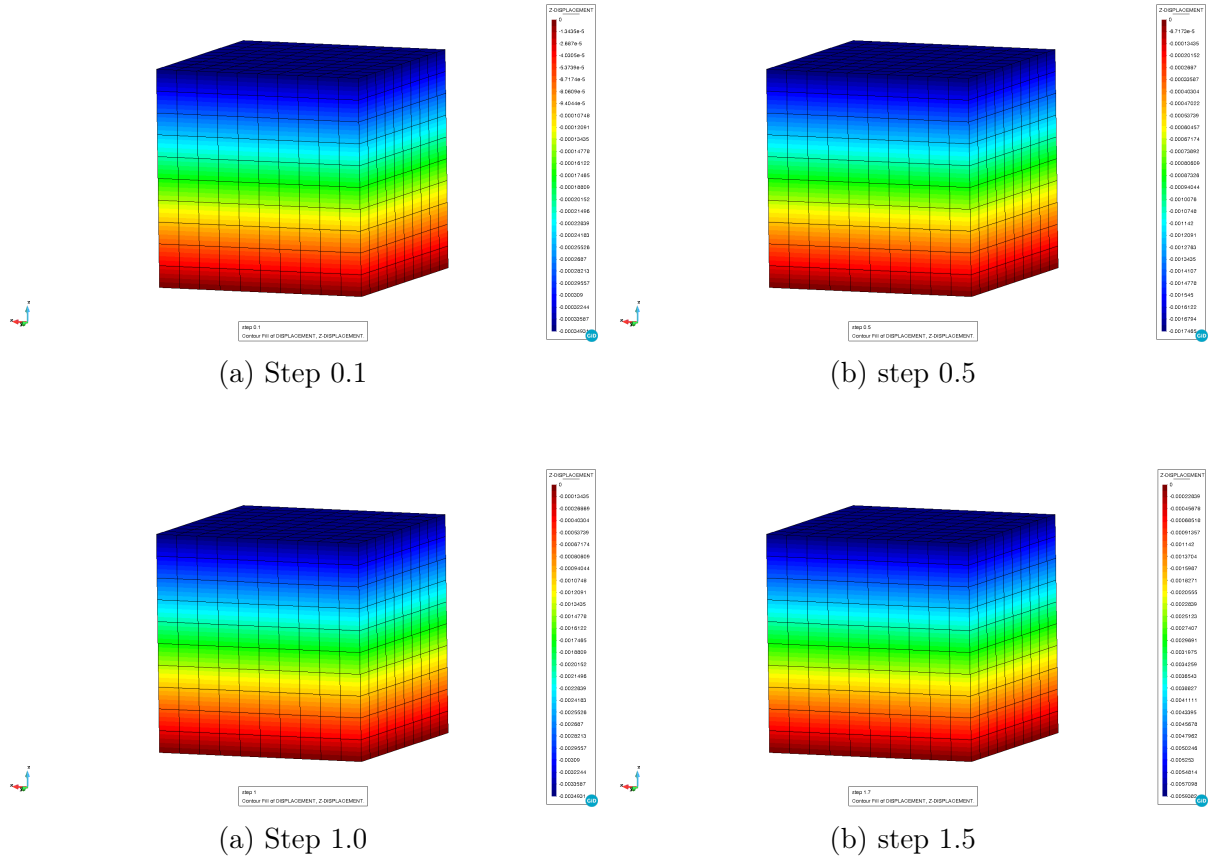


Figure 5.14: Z-axis displacements for different steps of the numerical model.

The stress-strain results are compared with those obtained in reference [41] so that the calibration of the material parameters is adequate. It can be seen that the elastic zone is adequately reproduced and the non-linear zone is stable compared to the experimental data which is consistent with the behavior of the numerical model, the instabilities of the experimental data will be discussed later. From this analysis we obtain the graph in Figure 5.15:

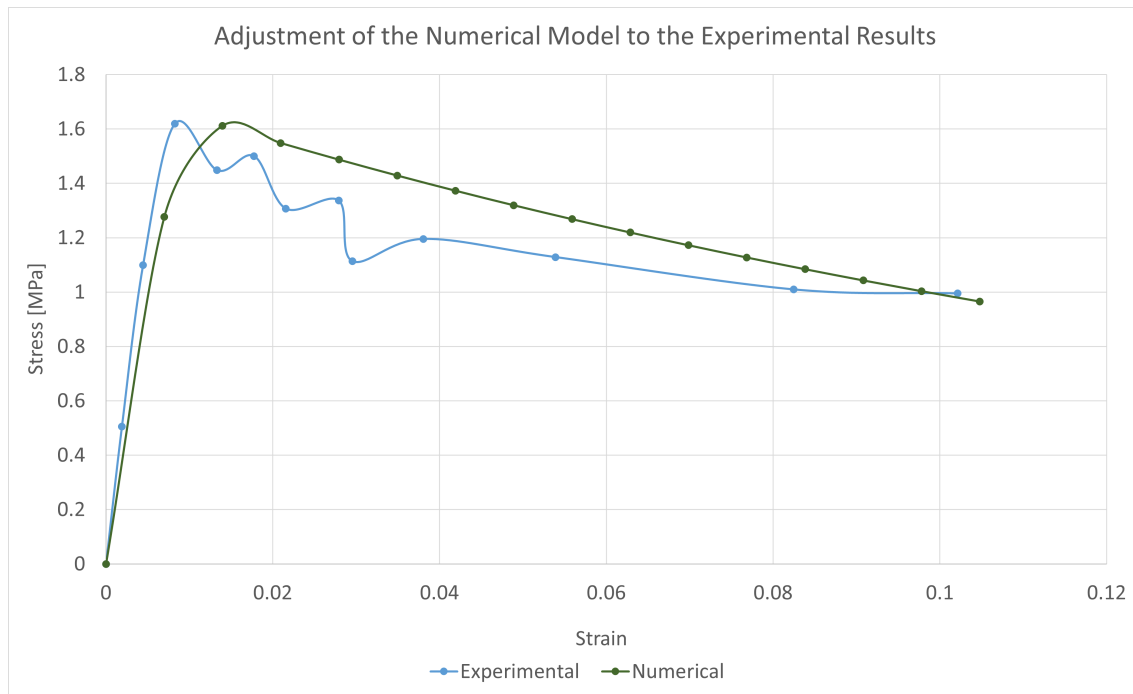


Figure 5.15: Results of the numerical model calibrating the composite material.

The final configuration of the component materials is shown in the following Table 5.7, these values differ from those obtained in the theoretical calculation of Equation (5.1), In the same way as in the previous case, it is the product of the large number of factors that can modify the properties of the organic fiber in its manufacturing process. This analysis will be addressed in the next section.

Material	Fiber [F]	Matrix [M]	Composite [C]
Tensile strength (MPa)	0.85	2.5	1.7
Young modulus (GPa)	0.33	1.2	0.77

Table 5.7: Calibrated mechanical properties of calculated component materials.

### 5.2.4 Results of the numerical characterization in tension

Once the materials have been calibrated, a numerical simulation of the tensile test is carried out based on the geometry described by Figure 5.11, in this case, due to the uncomplicated shape of the geometry, an unstructured mesh of tetrahedral elements was used, this in order to obtain a higher density of nodes.

The geometry of the specimen has a symmetry in the lateral plane in the X axis (see Figure 5.16), this allows to reduce the computational expense to be able to reduce the number of nodes of the model. the average size of the elements used is 2 mm.

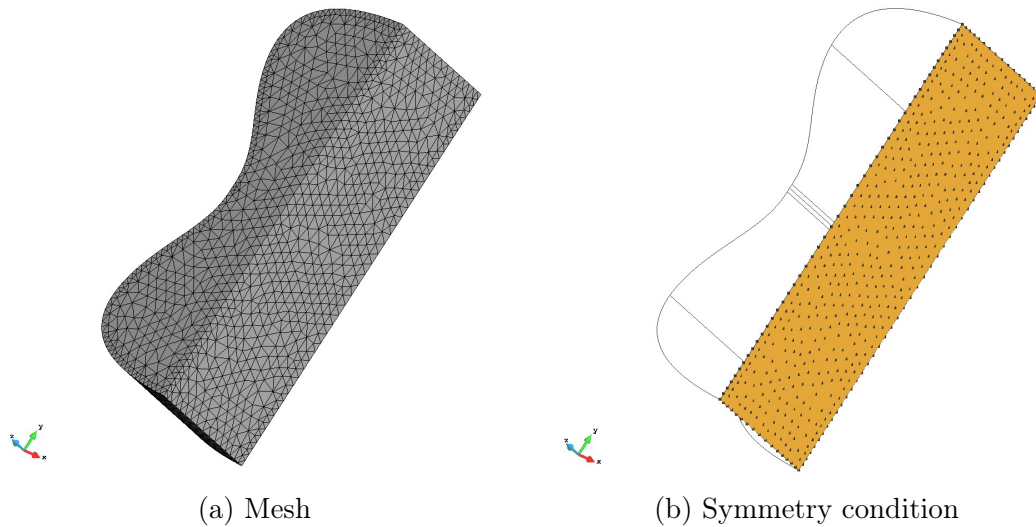


Figure 5.16: Mesh of tetrahedral elements with 7690 nodes

This model has two lateral edge conditions that represent the supports of the tongs with which the tensile test is performed (see Figure 5.17). In addition, it was necessary to use the Arc-length method and not the Newton-Raphson method to solve the system of equations, due to the fact that a constant displacement approach could not represent the experimental results.

Finally, and to rule out other sources of error, a mesh convergence analysis is performed, refining it to introduce the least possible error to the model due to the elements, the results of the different meshes in the traction model are presented in Figure 5.18, where they were compared with the experimental results of the author [41]. The evaluated meshes are presented in Table 5.8:

N <sup>o</sup> Mesh	N <sup>o</sup> Nodes	Maximum Stress [MPa]	Difference in %
Mesh 1	19851	0.296	0.0
Mesh 2	7690	0.289	2.4
Mesh 3	3035	0.266	23.6

Table 5.8: Comparison of maximum stress in the different meshes.

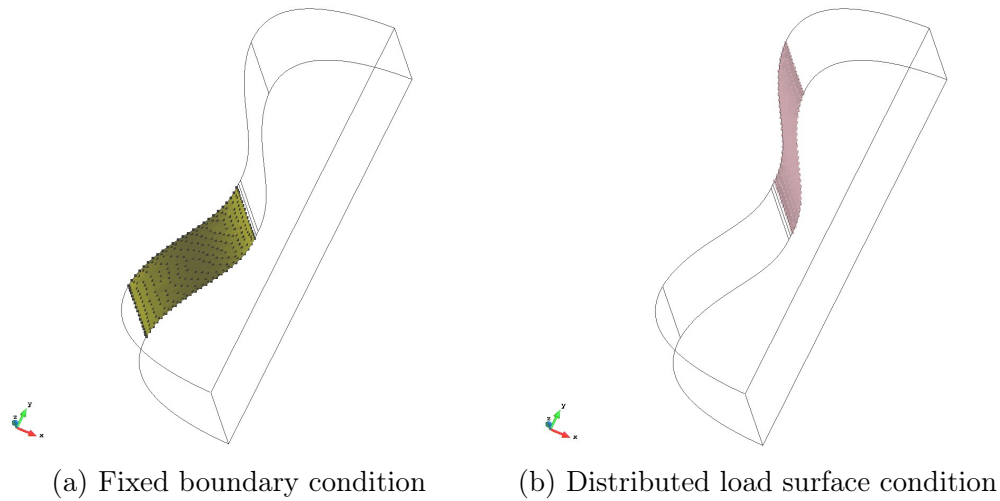


Figure 5.17: Boundary conditions in the numerical model.

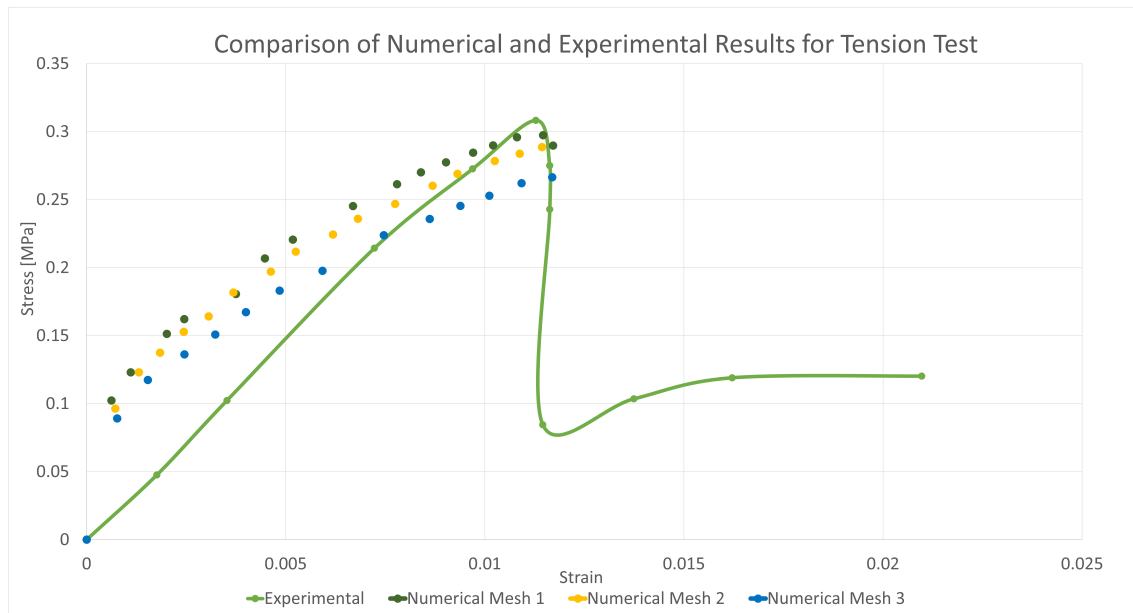


Figure 5.18: Validation of the numerical model with materials calibrated.

This model, like the others, considers the use of an isotropic behavior with damage, so we can evaluate the crack propagation in the numerical model. Due to the damage model, reaching the maximum stress, this value drops abruptly due to the fragility of the composite, this can be seen in Figure 5.20.

The solution of mesh number 2 is considered because the change in the result is only 2.4% and the increase in nodes is 150%, for this reason it is selected to reduce the computational expense of the numerical model. In this way, the final properties of the component materials are shown in Table 5.9, where only the compression property changes to tension. the behavior of foam concrete is more brittle, being an order of magnitude less than that of compression:

Material	Fiber [F]	Matrix [M]	Composite [C]
Tensile strength (MPa)	0.86	0.25	0.56
Young modulus (GPa)	0.085	0.25	0.17

Table 5.9: Calibrated mechanical properties of calculated component materials.

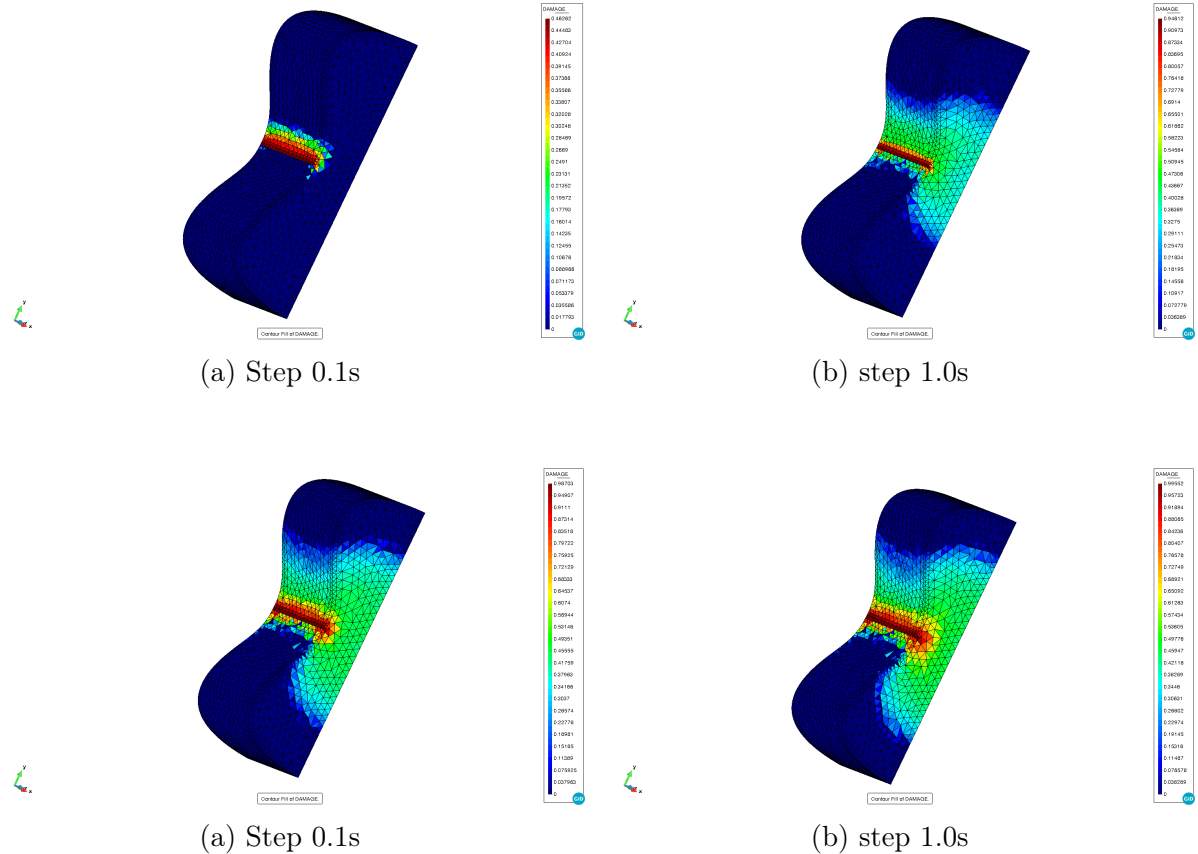


Figure 5.20: Damage result at different time steps.

## 5.2.5 Analysis of results

In the first stage of the numerical characterization of this compound, Newton-Raphson was used to solve the problem, which was able to obtain optimal results using the parallel RoM strategy. It can be seen that through the iterative process it was possible to adjust both the mechanical properties and the fracture energy of the material, obtaining the results of Figure 5.15.

The experimental results of the author [41] present an oscillation between the range of 0.02 to 0.04 of the Strain. The author explains that this is due to the fact that the test specimen fractured in such a way as to generate stacks of material that offered extra resistance while they fractured again (see Figure 5.10). This behavior is not appreciated in the numerical model because it is not possible to generate this physical interaction of over stacking. Despite this, the elastic range can be adjusted until material degradation begins.

After this, the "Dog-Bone" type specimen (Figure 5.11) was evaluated in a tensile test. This model was the most complex to study because the behavior of foamed concrete is very different between traction and compression. The bubbles or spaces found inside the concrete cause the tensile strength and crack propagation to be at very low loads, so the adjustment of the fracture energy was complex, despite this a difference close to order 2 for foamed cement between the numerical compression and traction models (See Table 5.10), values that are reasonable for this type of material.

<b>Fracture Energy [J/m<sup>2</sup>]</b>	<b>Fiber [F]</b>	<b>Matrix [M]</b>
Energy in compression	2.2E3	18E3
Energy in traction	45E1	95E1

Table 5.10: Fracture energies used in numerical models.

In this case, solving the system of equations of the model using Newton-Raphson did not provide optimal results, the specimen that considered a constant displacement was not able to represent the mechanical behavior of the reference experimental test, the use of this method gave a rupture of the material a 50% before the value obtained by the author [41]. For this reason, the use of an adaptive load surface was chosen, for which the calculation model was changed to Arc-Length. This model does manage to represent, together with the parallel RoM theory, the maximum stress of the Henequen fiber reinforced Foamed Concrete specimen.

Finally, a difference in Young's modulus was obtained between the experimental results and the calibrated numerical model. This difference can be mainly due to 2 reasons:

The first due to the difficulty of obtaining the properties of organic reinforcement fibers, due to the fact that there are more factors that can modify their mechanical properties during the manufacturing process. Some that stand out are: Amount of water inside the fibers, therefore the humidity of the environment is a critical parameter, quality of the plant that is used which affects a difference in the quality of the fiber and differences in the diameter of the fibers, because there is no mechanical equipment that can manufacture the fibers in a uniform and standardized way.

The combination of these aspects, together with the fact that the fiber is disperse, are factors that can cause the non-linear behavior of the compound to differ from the experimental and numerical ones. We can see in Figure 5.18, that the elastic range of the compound it ends around 0.0025 of the Strain, so the non-linear domain has a greater participation in these materials.

In this case, the lower control of the fiber properties and the differences in fiber density per matrix volume within the experimental specimen are sources of error that generate that the theoretical model cannot be adjusted in the same way as for the composite material. with oriented long fiber discussed above.

The second aspect is related to the foamed characteristic of the concrete. In the experimental compression test model, the spaces inside the material are broken, but due to the direction of the load, the material remains in contact while it is compressed, in the case of traction, the rupture of the air spaces generates that the crack propagate faster, this could explain that the numerical model starts with a higher stress than the experimental one, since the fiber in the numerical model has a greater influence than in the experimental one when it comes to supporting the tensile load due to the RoM parallel theory.

The numerical model approximates the properties of foamed concrete, but in the spaces inside the specimen, fibers that cannot be completely joined to the matrix can be grouped, causing their influence to decrease with respect to the numerical model.

Despite this, the results of the mesh refining and the material calibration are adequate, obtaining a result with a difference of 6.3% in the maximum stress with respect to the experimental one and a behavior of the crack that is physically possible and that is seen in the Figure 5.20, in addition to the fact that the fracture energy differs between tension and compression in standard orders of magnitude for concrete.



# Chapter 6

## Conclusions and Future work

### 6.1 Conclusions

In this work, a bibliographical study was presented to put in context the problem of composite materials and the importance of generating more studies for organic composite materials. This can be justified because they are materials that have a lower production cost and are the future for reducing the contamination in industries as important as aeronautics and the automotive industry. The contribution of this study is the realization of the complex numerical characterization of two composite materials reinforced by organic fibers using the SP-RoM theory. It has been possible to show the ability to work at a numerical level with this type of composite material and therefore show the ability to characterize it so that engineers can carry out mechanical design using FEA studies with these compounds, a fundamental aspect to promote the use of this type of materials. in the industry.

The conclusions of this work are divided into three fundamental aspects. The first one being that it is possible to carry out a correct numerical characterization of composite materials with organic fiber reinforcements using the SP-RoM theory in the Kratos Multiphysics calculation software. It was possible to evaluate the elastic and plastic zones of the materials until their fracture considering a non-linear behavior. The SP-RoM theory shows great robustness in the characterization of the mechanical properties of oriented long fiber composites, managing to reproduce with errors of less than 5%. For the case of dispersed fiber, the RoM parallel model manages to approximate the mechanical behavior of the compound considering the specific difficulty of reproducing the physical phenomenon that involves the use of foamed concrete as a matrix.

The second aspect is the importance of the correct use of resolution methods such as Newton-Raphson and Arc length in the study of materials. In this case for composite materials, a damage behavior for the fiber and the matrix was considered, so a Newton-Raphson solver with an imposed constant displacement is useful to approximate the solution. especially in cases where the deformation behavior is not complex, in these cases a constant displacement approach solved by N-R is sufficient to obtain good results.

On the other hand, when the load application is important due to specific boundary conditions or more complex behavior, applying a force control is impossible for N-R, this is because when considering a softening damage approach, when the force exceeds the maximum of the material, this solver cannot converge on solutions. This problem is solved using the Arc-Length solver because it can control the application of force, allowing the area of the curve after maximum stress to be recreated and approximating the area with damage. For this reason, this solver was applied to the Dog-Bone geometry specimen, due to the greater complexity of the mechanical behavior and the need to apply a constant force control and not a displacement control, since with the latter results were obtained with a error close to 50%.

The direct force application approach in result with used the Arc-Length model is robust enough to adequately resolve the mechanical behavior of the compound with an error of 6.3%. In addition, it is important to consider a good application of the flow rule implemented in fibers and matrices, since this allows establishing and adjusting the non-linear behavior that all composite materials present, being very robust the use of Initial Hardening Exponential Softening for long fibers and oriented.

Finally, a correct experimental study of the characterization of organic composite materials is fundamental. This is because they are materials that are more susceptible to external parameters that can alter the final mechanical properties of the composite. It is extremely important to consider aspects such as humidity and quality of the fibers at the time to manufacture these materials, in addition to a correct study of enough specimens to ensure their mechanical characteristics so later the numerical model can be adjusted in a better way.

## 6.2 Future work

There are other models to study conventional composite materials such as the Classical Laminate Theory and the Cohesive Zone Model. These models need to be tested again with organic composite materials, considering: reinforcements, matrices or both of natural origin with the objective to generate more information that may be available for the design and development of technological solutions using organic composite materials.

It was possible to see that the use of the parallel model is necessary to obtain a good modeling of short fiber composites, in this sense and to facilitate the use of these reinforcements, it is necessary to adapt the SP RoM to short fiber composites to use only one theory.

An adequate validation of the models with more experimental data is also important to verify the adequate reproduction of the physics involved in these composite materials.

Another point that should be taken into consideration is to study numerically other types of composite materials with organic reinforcements other than fibers, such as particle reinforcements or composite materials with complete layers of organic material, so as to see the responses of the models studied in this work.

Also, to implement an interface in Kratos Multiphysics for GiD specialized in composite materials with the purpose of promoting the study of these materials and facilitating their numerical analysis for researchers and engineers. -



# Bibliography

- [1] L. A. C. B.-M. A. Duval, A. Bourmaud. Influence of the sampling area of the stem on the mechanical properties of hemp fibers. *Letters, and undefined*, 2011.
- [2] R. W. A. O'Donnell, M.A. Dweib. Natural fiber composites with plant oil-based resin. *Composites Science and Technology*, 64:1135–1145, 2004.
- [3] B. Y.-M. A. Shalwan. In state of art: mechanical and tribological behaviour of polymeric composites based on natural fibres. *Design, and undefined*, 2013.
- [4] D. R. Aleksandra Konieczna, Aleksandra Rutkowska. Health risk of exposure to bisphenol a (bpa). *Department of Clinical and Experimental Endocrinology, Medical University of Gdańsk, Gdynia, Poland*, 2015.
- [5] M. A. G. Aranda. Ciencia de materiales, cuarto curso. *Universidad de Malaga*, 7:1–8, 2004.
- [6] N. ASTM. Standar test method for tensile properties of plastics. *D638-89*, 2022.
- [7] K. M. R. A.V. Ratna Prasad. Mechanical properties of natural fibre reinforced polyester composites: Jowar, sisal and bamboo. *Materials and Design*, 2011.
- [8] I. J. Azadeh Soroudi. Recycling of bioplastics, their blends and biocomposites: A review. *European Polymer Journal* 49, 2013.
- [9] B. C. Bourmaud A, Le Duigou A. What is the technical and environmental interest in reusing a recycled polypropylene-hemp fibre composite. *Polym Degrad Stab*, 96, 2011.
- [10] E. Car. Modelo constitutivo continuo para el estudio del comportamiento mecánico de los materiales. *Barcelona- Departament de Resistència de Materials i Estructures a l Enginyeria (RMEE)*, 2000.
- [11] CEMEX. Cemento cpc 30r extra data sheet. *Monterrey Mexico*, 2020.
- [12] P. Davvand, R. Rossi, M. Gil, X. Martorell, J. Cotela, E. Juanpere, S. Idelsohn, and E. Oñate. Migration of a generic multi-physics framework to hpc environments. *Computers and Fluids*, 80:301–309, 2013.
- [13] J. de Arespachaga Martínez. Glare: Caracterización mecánica y simulación numérica con kratos-multiphysics. *Escola Tècnica Superior d'Enginyers de Camins, Canals i Ports de Barcelona Universitat Politècnica de Catalunya, Departament de Enginyeria Civil i Ambiental*, 2011.

- [14] S. O. E. Car and E. Oñate. Tratamiento numérico de los materiales compuestos. *Barcelona- Monografía CIMNE*, 2000.
- [15] J. O. et al. “isotropic damage models and smeared crack analysis of concrete. *Second international conference on Computer Aided Analysis and Design of Concrete Structures*, 1990.
- [16] S. P. J. M. Fanran Meng, Yuanlong Cui. From aviation to aviation: Environmental and financial viability of closed-loop recycling of carbon fibre composite. *Composites Part B*, 108362:200, 2020.
- [17] B. D. L. R. Genuis S.J., Beeson S. Human excretion of bisphenol a: blood, urine, and sweat (bus) study. *j environ public health*. <http://www.ncbi.nlm.nih.gov/pmc/articles/PMC3504417/pdf/TSWJ2012-615068.pdf>, 2012.
- [18] S. M. M. W. Guigen Zhang, Helen Lu. 1.3.7 - composites. *Biomaterials Science An Introduction to Materials in Medicine*, 40:415–429, 2020.
- [19] N. P. M. T. H. Ku, H. Wang. A review on the tensile properties of natural fibre reinforced polymer composites. 2006.
- [20] E. Hinton and D. R. J. Owen. Introduction to finite elements computations. 1980.
- [21] S. S. M. H. H.Y. Sastra, J.P. Siregar. Tensile properties of arenga pinnata fiber-reinforced epoxy composites. *Polym.- Plast. Technol.Eng*, 2006.
- [22] A. S. I.A Lang, T.S Gallowey and W. Henley. Association of urinary bisphenol a concentration with medical disorders and laboratory abnormalities in adults. (*JAMA*) *The Journal of the American Medical Association*, 300, 2015.
- [23] H. W. C.-H. W. Jin Zhang, Venkata S. Chevali. Current status of carbon fibre and carbon fibre composites recycling. *Composites Part B*, 2020.
- [24] A. V.-G. P. J. H.-F. J. G. C. P. I. G.-C. Joaquin F. Castillo-Lara, Emmanuel A. Flores-Johnson and Q. M. Li. Mechanical properties of natural fiber reinforced foamed concrete. *Materials MDPI*, 2020.
- [25] M. R. H. Z. J.P. Siregar, S.M. Sapuan. Physical properties of short pineapple leaf fibre (palf) reinforced high impact polystyrene (hips) composites. *Adv. Compos. Lett.*, 2009.
- [26] A. P. N. K. Love Kerni, Sarbjeet Singh. A review on natural fiber reinforced composites. *Materials Today: Proceedings*, 2020.
- [27] C. K. K. Lovely Sabat. History of finite element method: A review. *Recent Developments in Sustainable Infrastructure*), 2020.
- [28] X. M. S. O. A. B. Lucia Gratiela Barbu, A Cornejo. Methodology for the analysis of post-tensioned structures using a constitutive serial-parallel rule of mixtures: Large scale non-linear analysis. *Composite structures*, 216:315–330, 2004.

- [29] J. J. Manso. Aprovechamiento integral de los composites fuera de uso. *Canales Sectoriales-<https://normas-apa.org/referencias/citar-pagina-web/>*, 2013.
- [30] L. I. Mauricio V. Donadon, Brian G. Falzona and J. M. Hodgkinson. A 3-d micromechanical model for predicting the elastic behaviour of woven laminates. *Composites Science and Technology, ISSN 0266-3538*, 2007.
- [31] O. E. R. J. J. Merlin Barschke, David Uribe and C. López. Finite element modeling of composite materials using kinematic constraints. *Ingeniería y Ciencia, ISSN 1794-9165*, 2009.
- [32] M.S.Huda, A. M. L.T. Drazal, and M. Misra. Natural-fiber composites in the automotive sector. *Michigan State University, USA, University of Calcutta, India and University of Guelph, Canada*, 7:222, 2008.
- [33] S. N.-C. P. A. A. N. Ranganathan, K. Oksman. Structure property relation of hybrid biocomposites based on jute, viscose and polypropylene: The effect of the fibre content and the length on the fracture toughness. 2016.
- [34] U. of Cambridge. Derivation of the rule of mixtures and inverse rule of mixtures. *Dissemination of IT for the Promotion of Materials Science*, 2022.
- [35] S. Oller. Nolinear dynamics of structures. 2014.
- [36] E. Oñate. Structural analysis with the finite element method. linear statics. volume 1. basis and solids. 2009.
- [37] R. R. P. Davvand and E. Oñate. An object-oriented environment for developing finite element codes for multi-disciplinary applications. *Arch. Computat. Methods Eng.*, 17:253-297, 2010.
- [38] S. T.-C. P. Joseph, K. Joseph. Effect of processing variables on the mechanical properties of sisal-fiberreinforced polypropylene composites. *science and Technology, and undefined*, 1999.
- [39] S. D. Petroudy. Physical and mechanical properties of natural fibers. *Faculty of New Technologies and Energy Engineering, Shahid Beheshti University, Mazandaran, Iran*, 3:60-78, 2017.
- [40] M. R. R. Sreenivasulu. Aero space applications of gfrp composites. *Mechanical Engineering Research (IJMER)*, 3:10-14, 2013.
- [41] E. I. S. R. G. Ramamurthy K, Kunhanandan N. A classification of studies on properties of foam concrete. *Cem. Concr. Compos*, 2009.
- [42] F. Rastellini. Modelación numérica de la no-linealidad constitutiva de laminados compuestos. 2006.
- [43] S. J. Reyes. Analysis of post-tensioned structures by means of a constitutive serial-parallel rule of mixtures. *Escola Técnica Superior d'Enginyers de Camins, Canals i Ports de Barcelona Universitat Politècnica de Catalunya*, 2018.

- [44] L. G. B. A. B. S. O. S Jiménez, A Cornejo. Failure pressure analysis of a nuclear reactor prestressed concrete containment building. *Engineering Structures*, 236:112052, 2021.
- [45] R. Serpieri. A novel constitutive model of composite materials with unidirectional long fibers: Theoretical aspects and computational issues. 2005.
- [46] A. M. E. M. G. G. Srebrenkoska V, Bogoeva Gaceva G. Recycling of polypropulene-based eco-composites. *Polym Int*, 57, 2008.
- [47] A. Tabiei and Y. Jiang. Woven fabric composite material model with material nonlinearity for nonlinear finite element simulation. *International Journal of Solids and Structures*, ISSN 0020-7683, 1999.
- [48] C. Trusdell and R. Toupin. The classical field theories. *Berlin- Springer Verlag*, 1960.
- [49] J. O. R. H. F. P. Veladez-Gonzales, A. Cervantes Uc. Effect of fiber surface treatment on the fiber-matrix bond strength of nature fiber reinforced composites. *Compos. PartB*, 1999.
- [50] A. C. Velázquez. A fully lagrangian formulation for fluid-structure interaction between free-surface flows and multi-fracturing solids and structures. *Doctoral Thesis, program in Structural Analysis, Dept. Civil and Environmental Engineering*, 2020.
- [51] K. S. Vilaplana F, Stromberg E. Environmental and resource aspects of sustainable biocomposites. *Polym Degrad Stab*, 95, 2010.
- [52] A. M. M. M.-C. P. B. W. Liu, L. Drzal. Influence of processing methods and fiber length on physical properties of kenaf fiber reinforced soy based biocomposites. *Engineering, and undefined*, 2007.
- [53] S. O. X. Martínez and F. Rastellini. Aplicaciones avanzadas de lso materiales compuestos en la obra civil y la edificación, capítulo 10 análisis no lineal de materiales compuestos mediante la teoría de mezcla serie paralelo. *OmniaScience*, 2014.